Journal Pre-proof

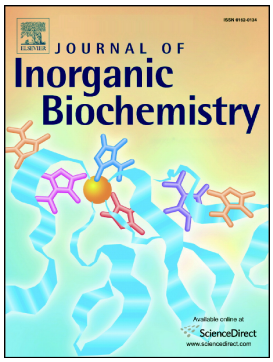

Aryl variation and anion effect on CT-DNA binding and in vitro biological studies of pyridinyl Ag(I) complexes

Adesola Abimbola Adeleke, Md. Shahidul Islam, Olakunle Sanni, Chunderika Mocktar, Sizwe J. Zamisa, Bernard Omondi

PII: S0162-0134(20)30294-4

DOI: https://doi.org/10.1016/j.jinorgbio.2020.111266

Reference: JIB 111266

To appear in: *Journal of Inorganic Biochemistry*

Received date: 30 April 2020

Revised date: 26 September 2020

Accepted date: 27 September 2020

Please cite this article as: A.A. Adeleke, M.S. Islam, O. Sanni, et al., Aryl variation and anion effect on CT-DNA binding and in vitro biological studies of pyridinyl Ag(I) complexes, *Journal of Inorganic Biochemistry* (2018), https://doi.org/10.1016/j.jinorgbio.2020.111266

This is a PDF file of an article that has undergone enhancements after acceptance, such as the addition of a cover page and metadata, and formatting for readability, but it is not yet the definitive version of record. This version will undergo additional copyediting, typesetting and review before it is published in its final form, but we are providing this version to give early visibility of the article. Please note that, during the production process, errors may be discovered which could affect the content, and all legal disclaimers that apply to the journal pertain.

© 2018 Published by Elsevier.

pyridinyl Ag(I) complexes

Adesola Abimbola Adeleke[1], Md. Shahidul Islam[2], Olakunle Sanni[2], Chunderika Mocktar[3] Sizwe J. Zamisa[4] and Bernard Omondi*[1]

[1] School of Chemistry and Physics, University of Kwazulu-Natal, Pietermaritzburg Campus, Private Bag X01, Scottsville 3209, South Africa

[2] Discipline of Biochemistry, School of Life Sciences, University of Kwazulu-Natal, Westville Campus, Private Bag X54001, Durban 4000, South Africa

[3] Discipline of Pharmaceutical Sciences, School of Health Sciences, University of Kwazulu-Natal, Westville Campus, Private Bag X54001, Durban 4000, South Africa

[4] School of Chemistry and Physics, University of Kwazulu-Natal, Westville Campus, Private Bag X54001, Westville 4001, South Africa

***Corresponding author.**

E-mail address: owaga@ukzn.ac.za http://orcid.org/0000-0002-3003-6712

Journal Pre-proof

Abstract

Synthesis and spectroscopic characterization of five ligands ((E)-2-((pyridin-2-ylmethylene)amino)phenol **L1,** 2-(pyridin-2-yl)benzo[d]thiazole **L2,** (E)-N-(2-fluorophenyl)-1-(pyridin-2-yl)methanimine **L3**, (E)-1-(pyridin-2-yl)-N-(p-tolyl)methanimine **L4** and (E)-1-(pyridin-2-yl)-N-(thiophen-2-ylmethyl)methanimine **L5** along with fifteen silver(I) complexes of **L1 – L5**, with a general formula $[AgL_2]^+X^-$ (L = Schiff base and X = NO_3^-, ClO_4^- or $CF_3SO_3^-$) is reported. The structures of complexes **[Ag(L4)$_2$]NO$_3$**, **[Ag(L5)$_2$]NO$_3$**, **[Ag(L3)$_2$]ClO$_4$**, **[Ag(L4)$_2$]ClO$_4$**, and **[Ag(L5)$_2$]CF$_3$SO$_3$** were determined unequivocally by single crystal X-ray diffraction analysis. calf-thymus deoxyribonucleic acid (CT-DNA), bovine serum albumin (BSA) binding studies, antioxidant, and antibacterial studies were performed for all complexes. Complexes **[Ag(L2)$_2$]NO$_3$**, **[Ag(L5)$_2$]NO$_3$**, **[Ag(L1)$_2$]ClO$_4$** and **[Ag(L3)$_2$]ClO$_4$** whose ligands have an OH^- and F^- as substituents or with a thiophene or thiazole moiety showed better antibacterial activities with lower minimum inhibitory concentration (MIC) values compared to the standard ciprofloxacin, against most of the bacterial strains tested. Similarly, complexes **[Ag(L1)$_2$]NO$_3$**, **[Ag(L2)$_2$]NO$_3$**, **[Ag(L3)$_2$]NO$_3$** and **[Ag(L5)$_2$]NO$_3$** with the NO_3^- anion, **[Ag(L1)$_2$]ClO$_4$** and **[Ag(L2)$_2$]ClO$_4$** with ClO_4^- anion, and **[Ag(L5)$_2$]CF$_3$SO$_3$** with $CF_3SO_3^-$ anion showed higher activities for antioxidant studies. Complexes **[Ag(L4)$_2$]ClO$_4$** and **[Ag(L4)$_2$]CF$_3$SO$_3$** with the Methyl substituent and $CF_3SO_3^-$ as the anion, displayed high antioxidant activities in FRAP (ferric reducing antioxidant power) than the standard ascorbic acid. Spectroscopic studies of all the

intercalation mode. In addition, the relatively moderate interaction of most of the complexes with BSA was through a static quenching mechanism.

Keywords: Ag(I) complexes, Pyridinyl Schiff bases, Antimicrobial, Antioxidant, DNA binding, protein binding.

Introduction

Schiff bases are an important class of ligands in coordination chemistry since they can easily be synthesised. They can also be electronically and sterically fine-tuned to stabilize various metal oxidation states. Schiff base ligands can accommodate acyl, aryl, and heteroaryl moieties making them excellent for transition metal complexation [1]. Heteroaryl with pharmacophores such as pyridine, [2, 3], and their derivatives can be found in over seven thousand already existing drugs [4]. In such Schiff bases, the pyridine moiety provides an extra N atom for coordination to metal ions in addition to the imine N atom and any other donor atoms such as O, S, and P that might be present on the ligand. This may lead to diverse modes of coordination with a transition metals, thereby providing an avenue for possible drug design [5].

Ag(I) complexes of Schiff bases have been widely studied due to their wide therapeutic applications and broad biological spectrum such as anticancer, antimicrobial, antioxidant, DNA and protein binding [6]. The choice for silver as antimicrobial agents has been based on their relatively low toxicity as compared to other transition metals and its ionic or chelated form exhibits tremendous biological activity [7]. Silver(I) sulfadiazine [8], for example, has been used in treating severe burns to prevent bacterial infections.

Several Ag(I) complexes [9-13] and their nanoparticles [14-16] have been reported for their antioxidant activity. Ag(I) complexes have shown to be effective scavengers of free radicals and reactive oxygen species (ROSs) which damage DNA, RNA, proteins, enzymes, and lipids, resulting in ailments and disorders such as diabetes mellitus, neurodegenerative diseases, rheumatoid arthritis, cataracts, cardiovascular diseases, respiratory diseases and aging to the human body [17]. Thus, the interaction of metal complexes with DNA and plasma proteins is important in the design of biologically active compounds [18]. The interaction of a complex with DNA may be via intercalation between base-pairs, electrostatic between cationic species and negatively charged DNA phosphate residues, or through major or minor grooves of the DNA via hydrogen bonding or van der Waals interactions [19-21]. It

Through studies involving interactions of protein to metal complexes, important information like the compound's distribution impact, concentration, metabolism, toxicity, and pharmaceutical kinetic in the bloodstream are obtained.

In continuation of our work on novel Ag(I) pyridinyl Schiff base complexes, we explored new ligands derived from thiophene-2-ylmethanamine, 2-fluoroaniline, p-toluidine, 2-aminophenol, and 2-aminobenzenethiol. We report herein the synthesis, characterization, and biological studies of *N,N*-bidentate pyridinyl Schiff base ligands, and their Ag(I) nitrate, perchlorate, and triflate complexes.

2. Experimental

2.1. Materials and instrumentation

Ethanol 99.5% (Aldrich, USA), diethyl ether 99.8% (Aldrich, USA), DMSO–*d6* 99.8% Merck, Germany), 2-pyridinecarboxaldehyde 99% (Aldrich, USA), 2-aminophenol >99% (Aldrich, USA), 2-aminobenzenethiol 99.5% (Aldrich, USA), 2-thiophenemethylamine >92% (Merck), *p*-toluidine 99.5% (Aldrich, USA), 2-fluoroaniline 99.5% (Aldrich, USA), dichloromethane 99% (Aldrich, USA), calf-thymus DNA (CT-DNA), ethidium bromide 95% (Aldrich, USA), bovine serum albumin 99% (Aldrich, USA), nitrogen gas, 5.0 technical grade (Air flex Industrial Gases, South Africa) were purchased from local suppliers. All chemicals were in analytical grade and used as received, while most of the solvents were dried using conventional techniques.

^{1}H NMR and ^{13}C NMR spectra were recorded on a BRUKER 400 MHz spectrometer in DMSO–*d6* and acetone *d6*. Chemical shift values are reported in parts per million (ppm) relative to the solvent residual peaks in DMSO-*d6* and acetone-*d6*; 2.5 and 2.05 ppm respectively for ^{1}H NMR and 39.5 and 29.4 ppm respectively for ^{13}C NMR. The splitting patterns in ^{1}H NMR spectra are reported as s for singlet, d for doublet, m for multiplet while J (the coupling constant is given in Hertz). The infrared spectra were recorded using a PerkinElmer Spectrum 100 FT-IR spectrometer, and the data are reported as percentage transmittances at the respective wavenumbers (cm^{-1}), between 4000 and 650 cm^{-1}. The mass spectra were recorded using Shimadzu LCMS-2020 instrument with only molecular ions (M^{+}) and major fragmentation peaks being reported with intensities quoted as percentages of the base peak. Elemental analyses were performed on Thermal-Scientific Flash 2000 CHNS/O analyzer. All melting points were determined using the Stuart Scientific melting

UV-1800 UV-Vis Spectrophotometer. The photoluminescence studies of CT-DNA and protein were recorded using PerkinElmer LS 45 Fluorescence spectrometer.

2.2. Synthesis of ligands

L1-L5 have been previously synthesised [23-28] but in this study, a slightly modified literature procedure [29] was employed in the pyridinyl Schiff base synthesis. To a hot solution of 2-pyridinecarboxaldehyde (0.091 mL, 1 mmol) in anhydrous ethanol (10 mL) was added to a hot solution of 2-aminophenol (1 mmol, 0.109 g) , 2-aminothiophenol (0.10 mL, 1 mmol), 2-fluoroaniline (0.097 mL, 1 mmol), p-toluidine (1 mmol, 0.11 g) and 2-thiophenemethylamine (1 mmol, 0.10 mL) respectively in anhydrous ethanol (10 mL) in the presence of glacial acetic acid. The resulting reaction was reflux at *ca.* 80 °C for 4 h. **L1**, **L2,** and **L4** solutions were evaporated to one-third of their initial volume under reduced pressure and ether (10 mL) was added to each solution to afford a precipitate. The precipitates were isolated via filtration, washed with cold ether (10 mL x 2), recrystallized from ethanol and dried over anhydrous $MgSO_4$. **L3** and **L5** solutions, on the other hand, were evaporated completely under pressure, the oil obtained was recrystallized from ethanol and dried over anhydrous $MgSO_4$.

2.3. Synthesis of Complexes

Complexes **1–15** were synthesized by dropwise addition of ethanolic solution (*ca.* 15 mL) of each of **L1–L5** (1 mmol) to an ethanolic (*ca.* 10 mL) solution of silver nitrate (0.5 mmol, *ca.* 0.085 g), silver perchlorate (0.5 mmol, *ca.* 0.10 g) and silver trifluoromethanesulfonate (0.5 mmol, *ca.* 0.13 g) respectively under constant stirring at dark. The reaction was carried out under nitrogen at ambient temperature for 6 h. The resulting precipitates were isolated using a vacuum filter. Afterward, the precipitates were washed with cold ethanol (10 mL X2) followed by cold ether (10 mL X2) and dried *in-vacuo.* The obtained complexes were recrystallized by dissolving the complexes in dichloromethane and layering with toluene.

2.3.1 *$[Ag(L1)_2]NO_3$* **1**

Brown, 0.38 g, 67 %, Melting point: 194–195 °C. ^{1}H-NMR (400 MHz, DMSO-*d6*, δ ppm): 10.04 (2H, d, *J* = 17.28 Hz, Hf-OH), 9.00 (2H, s, He-C=N-), 8.74 (2H, d, *J* =3.93 Hz, *H*d-Py), 8.17 (4H, m, Ha,b-Py), 7.73 (2H, t, *J* = 4.89, 4.66 Hz, Hc-Py), 7.43 (2H, d, *J* = 7.73 Hz, Hg-C_6H_4), 7.20 (2H, t, *J* = 7.72, 6.86 Hz, Hh-C_6H_4), 6.98 (2H, d, *J* = 8.22 Hz, Hj-C_6H_4), 6.89 (2H, t, *J* = 7.81, 7.40 Hz, Hi- C_6H_4). ^{13}C-NMR (400 MHz, DMSO-*d6*, 25 ℃): δ = 159.05 (C6-

Py), 129.27 (C10- C_6H_4), 127.98 (C3-Py), 127.69 (C1-Py), 121.81 (C8- C_6H_4), 119.93 (C9-C_6H_4), 116.90 (C11- C_6H_4). FT-IR (cm^{-1}); (OH) 3337, (Ar-CH) 3026, (-C=N-) 1622, (pyridyl) 1582. UV/Vis (CH_3CN): λ_{max} 321 nm. MS: *m/z* Calcd. for [$C_{24}H_{20}AgN_4O_2$]: 504.32; found $[Ag(L1)_2 + K + MeOH]^+$: 575 (12%), $[Ag(L1\text{-}OH)]^+$ 288 (100%). Anal. Calcd. (%) for ($C_{24}H_{20}AgN_5O_5$):. C, 50.90; H, 3.56; N, 12.37; found (%): C, 50.99; H, 3.58; N, 12.62.

2.3.2 *$[Ag(L2)_2]NO_3$* 2

Yellow solid, 0.40 g, 68 %, Melting point: 94–95 °C. ^{1}H-NMR (400 MHz, DMSO-*d6*, δ ppm): 8.74 (2H, d, *J* = 4.59 Hz, Hd-Py), 8.34 (2H, d, *J* = 7.87 Hz, Hh-C_6H_4), 8.18 (2H, d, *J* = 8.09 Hz, He-C_6H_4), 8.12 (2H, d, *J* = 8.09 Hz, Ha-Py), 8.05 (2H, m, Hb-Py), 7.59 (4H, m, Hg, f-C_6H_4), 7.51 (2H, t, *J* = 8.09, 7.00 Hz, Hc-Py). ^{13}C-NMR (400 MHz, DMSO-*d6*, 25 °C): δ = 168.90 (C5-Py), 153.60 (C7- C_6H_4), 150.16 (C6- C=N-), 150.00 (C4-Py), 137.95 (C2-Py), 135.33 (C8- C_6H_4), 126.66 (C11- C_6H_4), 126.19 (C10- C_6H_4), 126.01 (C1-Py), 123.28 (C9-C_6H_4), 122.57 (C12-C_6H_4), 120.53 (C3-Py). FT-IR (cm^{-1}): (Ar-CH) 3058, (C-S-C) 754, (pyridyl) 1584. UV/Vis (CH_3CN): λ_{max} 298 nm. MS: *m/z* Calcd. for [$C_{24}H_{16}AgN_4S_2$]: 532,41; found $[Ag(L2)_2 + H]^+$: 533 (100 %), $[Ag(L2) + CH_3CN + H]^+$: 359 (61%), Anal. Calcd. (%) for ($C_{24}H_{16}AgN_5O_3S_2$): C, 48.50; H, 2.71; N, 11.78; found (%): C, 48.46; H, 2.68; N, 11.73.

2.3.3 *$[Ag(L3)_2]NO_3$* 3

Green solid, 0.52 g, 92 %, Melting point: 84–85 °C, ^{1}H-NMR (400 MHz, DMSO-*d6*, δ ppm): 8.95 (2H, s, He-C=N), 8.80 (2H, d, *J* = 4.77 Hz, Hd-Py), 8.20 (2H, m, Hb-Py), 8.14 (2H, d, *J* = 7.28 Hz, Ha-Py), 7.77 (2H, m, Hh-C_6H_4), 7.48 (2H, m, Hc-Py), 7.30 (6H, m, Hi, g, f-C_6H_4). ^{13}C-NMR (400 MHz, DMSO-*d6*, 25 °C): δ = 162.57 (C6-C=N-), 151.20 (C12-C_6H_4), 150.37 (C5-Py), 149.94 (C4-Py), 139.09 (C2-Py), 137.06 (C7-C_6H_4), 128.95 (C10-C_6H_4), 127.96 (C3-Py), 127.85 (C9-C_6H_4), 125.14 (C8- C_6H_4). 122.32 (C1-Py), 116.42 (C11- C_6H_4). FT-IR (cm^{-1}): (Ar-CH) 3068, (-C=N-) 1626, (pyridyl) 1586, (C-F) 1490. UV/Vis (CH_3CN): λ_{max} 291 nm. MS: *m/z* Calcd. for [$C_{24}H_{18}AgF_2N_4$]: 508.30; found $[Ag(L3)_2 + H]^+$: 509 (100%). Anal. Calcd. (%) for ($C_{24}H_{18}AgF_2N_5O_3$): C, 50.55; H, 3.18; N, 12.28; found (%): C, 50.21; H, 3.05; N, 12.15.

2.3.4 [*$Ag(L4)_2]NO_3$* 4

Yellow solid, 0.51 g, 90 %, Melting point: 182–185 °C. ^{1}H-NMR (400 MHz, DMSO-*d6*, δ ppm): 8.79 (2H, s, He-CH=N-), 8.72 (2H, m, Hd-Py), 8.13 (2H, m, Ha-Py), 8.04 (2H, m, Hb-Py), 7.60 (2H, m, Hc-Py), 7.30 (4H, m, Hg-C_6H_4), 7.21 (4H, m, Hf-C_6H_4), 2.32 (6H, s, Hh-CH_3). ^{13}C-NMR (400 MHz, DMSO-*d6*, 25 °C): δ = 159.28 (C6-C=N-), 152.50 (C5-Py),

C12-C_6H_4), 126.40 (C3-Py), 123.98 (C1-Py), 121.49 (C8-C_6H_4, C13-C_6H_4), 20.57 (C11-CH_3), FT-IR (cm^{-1}): (Ar-CH) 3025, (-C=N-) 1623, (pyridyl) 1584, (C-CH_3) 2917. UV/Vis (CH_3CN): λ_{max} 292, 321 nm. MS: *m/z* Calcd. for [$C_{26}H_{24}AgN_4$]: 500,37; found [Ag(L4) + EtOH + CH_3CN]$^+$: 391 (8%), [$Ag(L4)_2$ + EtOH + CH_3CN + Na + H]$^+$: 611 (6%). Anal. Calcd. (%) for ($C_{26}H_{24}AgN_5O_3$): C, 55.53; H, 4.30; N, 12.45; found (%): C, 55.26; H, 4.19; N, 12.37.

2.3.5 *[Ag(L5)$_2$]NO$_3$* 5

Green solid, 0.60 g, 97 %, Melting point: 81–82 ^{o}C. ^{1}H-NMR (400 MHz, DMSO-*d6*, δ ppm): 8.79 (2H, s, He-CH=N), 8.46 (2H, m, Hd-Py), 8.13 (2H, m, Hb-Py), 7.94 (2H, d, *J* = 7.68 Hz, Ha-Py), 7.67 (2H, m, Hc-Py), 7.35 (2H, m, Hi-thio), 6.98 (2H, m, Hg-thio), 6.88 (2H, m, Hh-thio), 5.04 (4H, s, Hf-CH_2). ^{13}C-NMR (400 MHz, DMSO-*d6*, 25 °C): δ = 162.10 (C6- C=N-), 150.75 (C5-Py), 149.35 (C4-Py), 140.24 (C8-thio), 139.00 (C2-Py), 127.70 (C10-C_4H_3S), 127.32 (C9-C_4H_3S), 127.04 (C3-Py), 126.54 (C11-C_4H_3S), 125.96 (C1-Py), 57.31 (C7-CH_2). FT-IR (cm^{-1}): (Ar-CH) 3081, (-C=N-) 1639, (Pyridyl) 1588, (CH_2) 1435, (thiophene) 697. UV/Vis (CH_3CN): λ_{max} 289 nm. MS: *m/z* Calcd. for [$C_{22}H_{20}AgN_4S_2$]: 512,42; found [Ag(L5) + Lig. Frag.]$^+$: 400 (100%), 401 (28%), [$Ag(L5)_2$ + Lig. Frag. + EtOH + Na]$^+$: 691 (14%), 692 (7%). Anal. Calcd. (%) for ($C_{22}H_{20}AgN_5O_3S_2$. 0.25 C_3H_6O): C, 46.40; H, 3.68; N, 11.89; found (%): C, 46.22; H, 3.29; N, 11.65.

2.3.6 *[Ag(L1)$_2$]ClO$_4$* 6

Brown solid, 0.48 g, 79 %, Melting point: 147–148 ^{o}C. ^{1}H-NMR (400 MHz, DMSO-*d6*): δ ppm = 9.04 (2H, s, -C=N-), 8.63 (2H, d, *J* = 4.25 Hz, Hd-Py), 8.11 (2H, t, *J* = 7.04, 7.66 Hz Hb-Py), 8.00 (2H, d, *J* = 7.56 Hz, Ha-Py), 7.63 (2H, t, *J* = 7.15, 4.88 Hz, Hc-Py), 7.38 (2H, d, *J* = 7.73 Hz, Hj-C_6H_4), 7.14 (2H, t, *J* = 7.58, 7.44 Hz, Hh-C_6H_4), 6.84 (4H, t, *J* = 8.01, 5.00 Hz, Hi-C_6H_4). ^{13}C-NMR (400 MHz, DMSO-*d6*, 25 °C): δ = 158.72 (C6-C=N-), 151.10 (C5-Py), 150.81 (C12-C_6H_4), 150.41 (C4-Py), 138.87 (C7- C_6H_4), 135.60 (C2-Py), 128.94 (C10-C_6H_4), 127.65 (C3-Py), 127.36 (C1-Py), 121.48 (C8- C_6H_4), 119.60 (C9-C_6H_4), 116.57 (C11-C_6H_4). FT-IR(cm^{-1}); (OH) 3290, (-C=N-) 1624, (pyridyl) 1585. UV/Vis (CH_3CN): λ_{max} 291, 347, 357 nm. MS (ESI): *m/z* Calcd. for [$C_{24}H_{20}AgN_4O_2$]: 504.32; found [AgL-OH]$^+$: 288 (100%), [AgL + CH_3CN + H]$^+$ 346 (27%), [AgL + Lig. Frag. + Na]$^+$ 346 (47%), [$Ag(L1)_2$]$^+$ 503 (29 %). Anal. Calcd. (%) for ($C_{24}H_{20}AgClN_4O_6$): C, 47.74; H, 3.34; N, 9.28; found (%): C, 47.38; H, 3.08; N, 9.03.

White solid, 0.57 g, 90 %, Melting point: 195–196 °C. ^{1}H-NMR (400 MHz, DMSO-*d6*, δ ppm): 8.74 (2H, m, Hd-Py), 8.34 (2H, d, *J* = 7.87 Hz, Hh-C_6H_4), 8.17 (2H, d, *J* = 7.88 Hz, He-C_6H_4), 8.11 (2H, m, Ha-Py), 8.05 (2H, m, Hb-Py), 7.59 (4H, m, Hg, f-C_6H_4), 7.50 (2H, m, Hc-Py). ^{13}C-NMR (400 MHz, DMSO-*d6*, 25 °C): δ = 168.90 (C5-Py), 153.60 (C7-C_6H_4), 150.15 (C6-C=N-),150.01 (C4-Py), 137.96 (C2-Py), 135.33 (C8-C_6H_4), 126.67 (C11-C_6H_4), 126.20 (C10-C_6H_4), 126.02 (C1-Py), 123.29 (C9-C_6H_4), 122.57 (C12-C_6H_4), 120.57 (C3-Py). FT-IR (cm^{-1}): (Ar-CH) 3067, (thiazole-C=N-) 1490, 1318, (C-S-C) 760, (Pyridyl) 1585. UV/Vis (CH_3CN): λ_{max} 309 nm. MS: *m/z* Calcd. for [$C_{24}H_{16}AgN_4S_2$]: 532,41; found $[Ag(L2)_2+H]^+$: 533 (100%), $[Ag(L2) + CH_3CN + H]^+$ 362 (41%). Anal. Calcd. (%) for ($C_{24}H_{16}AgClN_4O_4S_2$): C, 45.62; H, 2.55; N, 8.87; found (%): C, 45.51; H, 2.48; N, 8.74.

2.3.8 *[Ag(L3)$_2$]ClO$_4$* **8**

Yellow solid, 0.58, 95 %, Melting point: 126–127 °C. ^{1}H-NMR (400 MHz, DMSO-*d6*, δ ppm): 8.94 (2H, s, He-CH=N), 8.80 (2H, m, Hd-Py), 8.17 (4H, m, Hb, a-Py), 7.76 (2H, m, Hh-C_6H_4), 7.47 (2H, m, Hc-Py), 7.30 (6H, m, Hf, g, i-C_6H_4). ^{13}C-NMR (400 MHz, DMSO-*d6*, 25 °C): δ = 162.53 (C6-C=N-), 153.69 (C12-C_6H_4), 151.22 (C5-Py), 149.94 (C4-Py), 139.10 (C2-Py), 128.96 (C7-C_6H_4), 127.96 (C10-C_6H_4), 125.15 (C3-Py), 125.11 (C9-C_6H_4), 122.29 (C2-Py), 122.06 (C1-Py), 116.47 (C11-C_6H_4). FT-IR (cm^{-1}): (Ar-CH) 3073, (-C=N-) 1625, (Pyridyl) 1584, (C-F) 1489. UV/Vis (CH_3CN): λ_{max} 292, 321 nm. MS: *m/z* Calcd. for [$C_{24}H_{18}AgF_2N_4$]: 508,30; found: [L3 + CH_3CN + Na]$^+$ 264 (100%), [$Ag(L3)_2$ + H]$^+$ 509 (98%). Anal. Calcd. (%) for ($C_{24}H_{15}AgClF_2N_4O_4$): C, 47.43; H, 2.99; N, 9.22; found (%): C, 47.32; H, 2.83; N, 9.02.

2.3.9 *[Ag(L4)$_2$]ClO$_4$* **9**

Yellow solid, 0.55 g, 92 %, Melting point: 210–211 °C. ^{1}H-NMR (400 MHz, DMSO-*d6*, δ ppm): 9.09 (2H, s, He-CH=N-), 8.78 (2H, m, Hd-Py), 8.22 (2H, m, Hb-Py), 8.11 (2H, m, Ha-Py), 7.76 (2H, m, Hc-Py), 7.41 (4H, m, Hg-C_6H_4), 7.23 (4H, m, Hf-C_6H_4), 2.30 (6H, s, Hh-CH_3). ^{13}C-NMR (400 MHz, DMSO-*d6*, 25 °C): δ = 158.98 (C6-C=N-), 151.54 (C5-Py), 150.35 (C4-Py), 145.73 (C7-C_6H_4), 139.59 (C10-C_6H_4), 138.35 (C2-Py), 130.24 (C9-C_6H_4 , C12-C_6H_4), 128.70 (C3-Py), 128.18 (C1-Py), 122.45 (C8-C_6H_4, C13-C_6H_4), 20.90 (C11-CH_3). FT-IR (cm^{-1}): (Ar-CH) 3028, (-C=N-) 1628, (Pyridyl) 1590. UV/Vis (CH_3CN): λ_{max} 290, 324 nm. MS: *m/z* Calcd. for [$C_{26}H_{24}AgN_4$]: 500,37; found [Ag(L4) + MeOH + Na]$^+$ 359 (100%), $[Ag(L4)_2 + H]^+$ 501 (67%). Anal. Calcd. (%) for ($C_{26}H_{24}AgClN_4O_4$): C, 52.06; H, 4.03; N, 9.34; found (%): C, 51.86; H, 3.78; N, 9.28.

Brown, 0.35 g, 57 %, Melting point: 155-156°C. ^{1}H-NMR (400 MHz, DMSO-*d6*, δ ppm): 8.74 (2H, s, He-CH=N), 8.56 (2H, d, *J* = 4.26 Hz Hd-Py), 8.10 (2H, m, Hb-Py), 7.94 (2H, d, *J* = 7.77 Hz, Ha-Py), 7.67 (2H, m, Hc-Py), 7.41 (2H, d, *J* = 5.06 Hz, Hi-thio), 7.04 (2H, m, *J* = 3.34 Hz, Hg-thio), 6.95 (2H, m, Hh-thio), 5.06 (4H, s, Hf-CH_2). ^{13}C-NMR (400 MHz, DMSO-*d6*, 25 °C): δ = 162.32 (C6-C=N-), 150.60 (C5-Py), 149.83 (C4-Py), 140.41 (C8-C_4H_3S), 138.80 (C2-Py), 127.46 (C10-C_4H_3S), 127.11 (C9-C_4H_3S), 126.58 (C3-Py), 126.42 (C11-thio), 125.91 (C1-Py), 57.42 (C7- CH_2). FT-IR (cm^{-1}): (Ar-CH) 3079, (Pyridyl) 1593, (thiophene) 705. UV/Vis (CH_3CN): λ_{max} 291 nm. MS: *m/z* Calcd. for [$C_{22}H_{20}AgN_4S_2$]: 512.42; found [$Ag(L5)_2$ + Lig. Frag.]$^+$ 613 (100%). Anal. Calcd. (%) for ($C_{22}H_{20}AgClN_4O_4S_2$. 0.25 C_3H_6O): C, 43.62; H, 3.46; N, 8.94; found (%): C, 43.64; H, 3.68; N, 8.68.

2.3.11 *[Ag(L1)$_2$]CF$_3$SO$_3$* 11

Brown, 0.62 g, 95 %, Melting point: 137-138 °C. ^{1}H-NMR (400 MHz, DMSO-*d6*): δ ppm = 9.96 (2H, s, Hf-OH), 9.05 (2H, s, He-C=N-), 8.68 (2H, d, *J* = 4.77 Hz, *H*d-Py), 8.16 (4H, m, Ha,b-Py),7.69 (2H, m, Hc-Py), 7.39 (2H, m, Hg-C_6H_4), 7.17 (2H, m, Hh- C_6H_4), 6.94 (2H, m, Hj-C_6H_4), 6.87 (2H, m, Hi- C_6H_4). ^{13}C-NMR (400 MHz, DMSO-*d6*, 25 °C): δ = 158.84 (C6-C=N-), 151.26 (C5-Py), 150.68 (C11-C_6H_4), 150.38 (C4-Py), 138.64 (C7- C_6H_4), 137.84 (C2-Py), 128.98 (C10- C_6H_4), 128.56 (C3-Py), 127.15 (C1-Py), 121.18 (C8- C_6H_4), 119.73 (C9-C_6H_4), 116.60 (C11- C_6H_4). FT-IR (cm^{-1}); (OH) 3251, (Ar-CH) 3060, (-C=N-) 1623, (pyridyl) 1587. UV/Vis (CH_3CN): λ_{max} 292, 347, 358 nm. MS (ESI): *m/z* Calcd. for [$C_{24}H_{20}AgN_4O_2$]: 503.06; found [AgL1-OH]$^+$: 288 (100%), [AgL1 + CH_3CN + H]$^+$ 346 (29%), [AgL1 + Frag. + Na]$^+$ 346 (29%), [$Ag(L1)_2$]$^+$ 503 (29 %). Anal. Calcd. (%) for ($C_{25}H_{20}AgF_3N_4O_5S$. 0.25 C_3H_6O): C, 46.31; H, 3.24; N, 8.39; found (%): C, 46.72; H, 3.18; N, 8.67.

2.3.12 *[Ag(L2)$_2$]CF$_3$SO$_3$* 12

Orange solid, 0.48 g, 70 %, Decomposes at 183–184 °C, ^{1}H-NMR (400 MHz, DMSO-*d6*, δ ppm): 8.73 (2H, m, Hd-Py), 8.34 (2H, m, Hh-C_6H_4), 8.18 (2H, m, He-C_6H_4), 8.11 (2H, m, Ha-Py), 8.05 (2H, m, Hb-Py), 7.60 (2H, m, Hg-C_6H_4), 7.56 (2H, m, Hf-C_6H_4), 7.50 (2H, m, Hc-Py). ^{13}C-NMR (400 MHz, DMSO-*d6*, 25 °C): δ = 169.92 (C5-Py), 158.86 (C7-C_6H_4), 152.92 (C6-C=N-),148.49 (C4-Py), 137.86 (C2-Py), 135.99 (C8-C_6H_4), 135.36 (C11-C_6H_4), 126.13 (C10-C_6H_4), 125.02 (C1-Py), 123.27 (C9-C_6H_4), 119.61 (C12-C_6H_4), 119.03 (C3-Py). FT-IR (cm^{-1}): (Ar-CH) 3065, (thiazole-C=N-) 1461, 1376, (C-S-C) 762, (Pyridyl) 1588. UV/Vis (CH_3CN): λ_{max} 300 nm. MS: *m/z* Calcd. for [$C_{24}H_{16}AgN_4S_2$]: 532,41; found [$Ag(L2)_2$

found (%): C, 43.73; H, 1.95; N, 8.02

2.3.13 *[Ag(L3)$_2$]CF$_3$SO$_3$* 13

Green, 0.53, 81 %, Melting point: 106-107 °C. ^{1}H-NMR (400 MHz, DMSO-*d6*, δ ppm): 8.98 (2H, s, He-CH=N), 8.81 (2H, m, Hd-Py), 8.22 (4H, m, Hb-Py), 8.14 (2H, d, Ha-Py), 7.78 (2H, m, Hh-C_6H_4), 7.48 (2H, m, Hc-Py), 7.29 (6H, m, Hf, g, i-C_6H_4). ^{13}C-NMR (400 MHz, DMSO-*d6*, 25 °C): δ = 162.47 (C6-C=N-), 153.71 (C12-C_6H_4), 151.33 (C5-Py), 149.64 (C4-Py), 139.26 (C2-Py), 129.03 (C7-C_6H_4), 128.40 (C10-C_6H_4), 128.12 (C3-Py), 125.10 (C9-C_6H_4), 122.33 (C8-C_6H_4). 122.21 (C1-Py), 116.46 (C11-C_6H_4). FT-IR (cm^{-1}): (Ar-CH) 3068, (-C=N-) 1628, (Pyridyl) 1588, (C-F) 1491. UV/Vis (CH_3CN): λ_{max} 290 nm. MS: *m/z* Calcd. for [$C_{24}H_{18}AgF_2N_4$]: 508,30; found [Ag(L3)$_2$ + H]$^+$: 509 (24%). Anal. Calcd. (%) for ($C_{25}H_{18}AgF_5N_4O_3S$): C, 45.68; H, 2.76; N, 8.52; found (%): C, 46.01; H, 2.83; N, 8.72.

2.3.14 *[Ag(L4)$_2$]CF$_3$SO$_3$* 14

Yellow solid, 0.46 g, 71 %, Melting point: 99–101 °C. ^{1}H-NMR (400 MHz, DMSO-*d6*, δ ppm): 9.05 (2H, s, He-CH=N-), 8.78 (2H, m, Hd-Py), 8.21 (2H, m, Hb-Py), 8.12 (2H, m, Ha-Py), 7.75 (2H, m, Hc-Py), 7.39 (4H, m, Hg-C_6H_4), 7.23 (4H, m, Hf-C_6H_4), 2.30 (6H, s, Hh-CH_3). ^{13}C-NMR (400 MHz, DMSO-*d6*, 25 °C): δ = 159.04 (C6-C=N-), 151.46 (C5-Py), 150.57 (C4-Py), 145.85 (C7-C_6H_4) 129.46 (C10-C_6H_4), 138.24 (C2-Py), 130.23 (C9-C_6H_4 ,C12-C_6H_4), 128.31 (C3-Py), 126.24 (C1-Py), 122.38 (C8-C_6H_4, C13-C_6H_4), 20.89 (C11-CH_3), FT-IR (cm^{-1}): (Ar-CH) 3025, (-C=N-) 1626, (Pyridyl) 1587, (C-CH_3) 2917. UV/Vis (CH_3CN): λ_{max} 290, 321 nm. MS : *m/z* Calcd. for [$C_{26}H_{24}AgN_4$]: 500,37; found [Ag(L4)$_2$ + H]$^+$ 501 (100%). Anal. Calcd. (%) for ($C_{27}H_{24}AgF_3N_4O_3S$): C, 49.94; H, 3.73; N, 8.63; found (%): C, 49.67; H, 3.38; N, 8.49.

2.3.15 *[Ag(L5)$_2$]CF$_3$SO$_3$* 15

Green solid, 0.58 g, 87 %, Melting point: 97–98 °C. ^{1}H-NMR (400 MHz, DMSO-*d6*, δ ppm): 8.79 (2H, s, He-CH=N), 8.47 (2H, m, Hd-Py), 8.13 (2H, m, Hb-Py), 7.94 (2H, d, *J* = 7.43 Hz, Ha-Py), 7.68 (2H, m, Hc-Py), 7.34 (2H, m, Hi-thio), 6.98 (2H, m, Hg-thio), 6.88 (2H, m, Hh-thio), 5.03 (4H, s, Hf-CH_2). ^{13}C-NMR (400 MHz, DMSO-*d6*, 25 °C): δ = 162.36 (C6- C=N-), 156.15 (C5-Py), 150.72 (C4-Py), 140.57 (C8-C_4H_3S), 138.92 (C2-Py), 127.59 (C10-C_4H_3S), 127.23 (C9-C_4H_3S), 126.57 (C3-Py), 126.01 (C11-C_4H_3S), 125.27 (C1-Py), 57.57 (C7-CH_2). FT-IR (cm^{-1}): (Ar-CH) 3077, (-C=N-) 1622, (Pyridyl) 1591, (CH_2) 1474, (thiophene) 703. UV/Vis (CH_3CN): λ_{max} 290 nm. MS : *m/z* Calcd. for [$C_{22}H_{20}AgN_4S_2$]: 512.42; found

($C_{23}H_{20}AgF_3N_4O_3S_3$): C, 41.76; H, 3.05; N, 8.47; found (%): C, 41.72; H, 2.96; N, 8.27.

2.4 Single-crystal X-ray diffraction

Crystal evaluation and data collection of **4**, **5**, **8**, **9,** and **15** were recorded on a Bruker Apex Duo diffractometer equipped with an Oxford Instruments Cryojet operating at 100(2) K and an Incoatec microsource operating at 30 W power. The data were collected with Mo Kα (λ = 0.71073 Å) radiation at a crystal-to-detector distance of 50 mm using omega and phi scans. The data were reduced with the programme SAINT [30] using outlier rejection, scan speed scaling, as well as standard Lorentz and polarisation correction factors. A SADABS [31] semi-empirical multi-scan absorption correction was applied to the data.

The structures of **4**, **5**, **8**, **9,** and **15** were solved by the direct method using the SHELXS [32] program and refined. The visual crystal structure information was performed using ORTEP-3 [33], system software. Non-hydrogen atoms were first refined isotropically and then by anisotropic refinement with a full-matrix least-squares method based on F^2 using SHELXL [34]. All hydrogen atoms were positioned geometrically, allowed to ride on their parent atoms, and refined isotropically. The crystallographic data and structure refinement parameters for **4**, **5**, **8**, **9,** and **15** are given in **Table 1**.

Complex **4** is a two component, non-merohedral twin. An HKLF5 data refinement revealled a mass ratio of 0.741(15):0.259(15) with a twin matrix -1 0 0 0 -1 0 0 0 -1. A disorder was observed in **5, 9** and **15**. The anionic molecular species is severely disordered in **5** because it resides in voids that form channels between the cationic Ag(I) complexes as depicted in Fig. S1 (see supplementary info). Attempts to model the disordered ion was unsuccessful and the contribution of the missing solvent to the calculated structure factors was taken into account by using a SQUEEZE [35] routine of PLATON [36]. A solvent mask was calculated, and 204 electrons were found in a volume of 540 $Å^3$ in 1 void per unit cell. This is consistent with the presence of 1.5[NO_3] per Asymmetric Unit which accounts for 186 electrons per unit cell. In **9**, one of the perchlorate ions is disordered over a special position. PART -1 and -2 instructions were used to model the disorder with all components having equal site occupancy factor. The triflate ion is also disordered over a special position in **15** and PART -1 instruction and 50% site occupancy was used to model the disordered anion.

Table 1: Crystal data and structure refinement for complexes 4, 5, 8, 9 and 15

	4	**5**	**8**	**9**	**15**
Chemical formula	$C_{52}H_{50}Ag_2N_{10}O_7$	$C_{22}H_{20}AgN_4S_2$	$C_{24}H_{18}AgF_2N_4{\cdot}ClO_4$	$C_{26}H_{24}AgClN_4O_4$	$C_{23}H_{22}AgF_3N_4O_4S_3$
Formula Weight	1142.76	512.41	607.74	599.81	679.49
Crystal system	Monoclinic	Monoclinic	Monoclinic	Monoclinic	Monoclinic
Space group	*Pn*	*I*2/*a*	*C*2/*c*	*C*2/*c*	*I*2/*c*
a(Å)	11.6045(7)	11.4202(2)	18.988(2)	25.8553(14)	11.5656(8)
b(Å)	17.0924(10)	15.9615(3)	5.9799(7)	15.9354(14)	15.4463(11)
c(Å)	12.4183(7)	13.5887(3)	13.8799(15)	19.6875(12)	15.1331(10)
α(°)	90	90	90	90	90
β(°)	102.270(2)	101.925(2)	130.737(4)	111.464(4)	107.439(3)
γ(°)	90	90	90	90	90
V(Å^3)	2406.9(2)	2423.54(8)	1194.2(2)	75[illegible].0(9)	2579.2(3)
Z	2	4	2	12	4
ρ_{calc}(gcm^{-3})	1.577	1.404	1.690	1.583	1.750
μ (mm^{-1})	0.879	1.02	1.011	0.947	1.09
F(000)	1164		608	3648	1368
Crystal size (mm^3)	0.40 x 0.18 x 0.17	0.40× 0.30 × 0.20	0.24 × 0.10 × 0.04	0.37 x 0.28 x 0.22	0.30 × 0.20 × 0.10
θ range for data collection (°)	2.4 to 56.5	4.5 to 56.8	3.9 to 56.4	3.1 to 55.0	1.9 to 28.2
Reflections collected	44935	13183	0381	65342	21898
Independent reflections	10584 [R(int) = 0.029]	2985 [R(int) = 0.016]	2583 [R(int) = 0.018]	8598 [R(int) = 0.027]	3195 [R(int) = 0.024]
Data / restraints / parameters	10584 /321 / 792	2985/0/152	2583 / 1 / 164	8598 / 0 / 509	3195 / 164 / 216
R indices [I>2sigma(I)]	R1 = 0.022	R[illegible] = 0.026	R1 = 0.018	R1 = 0.027	R1 = 0.036
	wR2 = 0.051	wR_2 = 0.063	wR2 = 0.043	wR2 = 0.065	wR2 = 0.094
R indices (all data)	R1 = 0.024	R_1 = 0.027	R1 = 0.019	R1 = 0.033	R1 = 0.037
	wR2 = 0.052	wR_2 = 0.064	wR2 = 0.043	wR2 = 0.069	wR2 = 0.095
Largest diff. peak and hole (e Å^{-3})	0.46 and -0.33	0.39 and -0.56	0.54 and -0.29	1.08 and -0.63	1.80 and -0.72

Journal Pre-proof

2.5.1 *Müeller-Hinton agar test plates preparation*

Sterilized Nutrient agar medium was first prepared by dissolving 38 g of Müeller-Hinton agar (MHA) (Biolab, South Africa) in distilled water (1 L). The resulting Nutrient agar medium was subjected to sterilization by autoclaving for 15 min at 121 °C and then cooled down to 45 °C in a water bath. The cooled Agar medium was poured in Petri dishes, while ensuring a uniform 4 mm depth of the medium and cooling further to ambient temperature [29].

2.5.2 *Inoculation procedure*

Complexes **1–15** and their ligands were tested against four gram-negative bacteria; *Salmonella typhimurium* ATCC 14026, *Pseudomonas aeruginosa* ATCC 27853, *Escherichia coli* ATCC 25922 and *Klebsiella pneumoniae* ATCC 31488 and two gram-positive bacteria, viz: *Staphylococcus aureus* ATCC 700699 (methicillin-resistant) and *Staphylococcus aureus* ATCC 25923. These bacteria were inoculated in a sterilized Nutrient Broth (NB) (Biolab, South Africa) through streak plate technique and incubated at 37 °C for 18 h. The nutrient broth was sterilized by dissolving 1.3 g in distilled water (100 mL). *Ca.* 10 mL of the nutrient broth was transferred into a cotton wool-plugged test tubes and wrapped with an aluminium foil. The nutrient broth in the test tubes was then autoclaved for 15 min at 121 °C and cooled to 37 °C. Following this was the isolation of a single colony of the bacteria and inoculated into a 10 mL sterile NB which was then incubated in a shaking incubator at 37 °C for 18 h. Each of the bacteria strain concentrations was adjusted with sterile distilled water to get a final concentration of 1.5 x 10^8 cfu/mL, i.e., 0.5 Mc Farland's Standard using a densitometer (Mc Farland Latvia) [37]. The bacteria were lawn inoculated on the set MHA Petri-dishes using a sterile cotton swab. Screening of **L1–L5** and **1–15** for antibacterial activity was first carried out by spotting 5 µL of their solution (prepared from the dissolution of 1000 µg of the **L1–L5** and **1–15** in 1 mL dimethyl sulfoxide (DMSO) on an MHA petri dish and incubated at 37 °C for 18 h. The antibacterial activity was determined by looking out for a clear zone at the spotting point. The compounds with potential antimicrobial activity were then tested for their minimum inhibitory concentration (MIC) against six bacterial. 10 serial dilution of **L1–L5** and **1–15** was done to obtain 1000 µg/mL to 0.2 µg/mL concentrations, where the compounds showed lower MICs than 0.2 µg/mL, the solution was further diluted 5 times to obtain 0.100 µg/mL to 0.00625 µg/mL concentrations. Evaluation of the compounds MIC was determined by spotting 5 µL of each concentration of **L1–L5** and **1–15** on the MHA plates, and the plates were incubated at 37 °C for 18 h. These procedures were done in triplicate to give the accurate lowest concentration of the compounds where no visible

as a negative control [37-39].

2.6 Antioxidant assay

Antioxidant activity studies of **L1–L5** and **1–15** was done using two assays; Free radical scavenging and Ferric reducing antioxidant power (FRAP) assay.

The free radical scavenging ability of **L1–L5** and **1–15** was determined using the 2,2-diphenyl-1-picrylhydrazyl (DPPH) method following a procedure by Liyana-Pathirana *et al.* [40]. Briefly, a 500 µL of 0.3 mM DPPH solution was mixed with 1 mL of different concentrations (0.25 mg/mL, 0.5 mg/mL, 1 mg/mL and 2 mg/mL) of the **L1–L5** and **1–15**. Various concentrations of Ascorbic acid (0.25 mg/mL, 0.5 mg/mL, 1 mg/mL and 2 mg/mL) were used as reference material. The mixture was vortexed thoroughly and kept in the dark at room temperature for 30 min. Then the absorbances were measured at 517 nm after 30 min of incubation at room temperature to evaluate the DPPH reduction. **L1–L5** and **1–15** ability to scavenge DPPH radical was calculated by the formula as shown in Equation 1.

$$\%\, Scavenging\ Activity\ = Absorbance\ of\ \frac{Control - Sample}{Control} \times 100 \quad (1)$$

The ferric reducing antioxidant power assay is often used to evaluate the ability of an antioxidant to donate an electron. The reducing ability of the compounds was measured using a previously published method [41] after slight modifications where different concentrations (0.25 mg/mL, 0.5 mg/mL, 1 mg/mL and 2 mg/mL) of **L1–L5** and **1–15** and standard (Ascorbic acid) were mixed with 2.5 mL of phosphate buffer (0.2 mol/L, pH 6.6) and 2.5 mL of 1% w/v potassium ferricyanide respectively. The resulting mixture was incubated at 50 °C for 20 min, and 2.5 mL of 10% trichloroacetic acid was added to acidify the mixture. After that, 1 mL of the acidified mixture was added to 1 mL of distilled water and 0.5 mL of 0.1% $FeCl_3$. The absorbance of the resulting solution was then measured at 700 nm. The antioxidant power of the compounds was expressed as a percentage of ferric reducing antioxidant power Ascorbic acid equivalent, as shown in Equation 2.

$$\%\, FRAP\ = Absorbance\ of\ \frac{Absorbance\ of\ Sample}{Absorbance\ of\ Ascorbic\ Acid} \times 100 \quad (2)$$

The interaction of the **L1–L5** and complexes **1–15** with calf thymus-DNA was carried out in a Phosphate buffer saline solution pH 7.2 stored at 4 °C. The DNA stock solution was prepared by dissolving CT-DNA sodium salt in Phosphate buffer saline solution with continuous stirring overnight. It was filtered and stored at 4 °C and used within four days. The final concentration of CT-DNA sodium salt was determined by UV-visible absorption using the absorption coefficient ε260 = 6600 M^{-1} cm^{-1} [42]. The ratio of CT-DNA at 260 and 280 nm UV absorbance was 1.93, indicating that it is pure and sufficiently free of protein contamination. A fixed amount of the compounds (50 µM) were prepared by dissolving an appropriate amount in DMSO.

2.7.1 *DNA Absorption spectral study*

The absorption study was done by titrating different concentrations of CT-DNA (0–30 µM) in phosphate buffer saline solution against constant concentrations (50 µM) of **L1–L5** and **1–15.** The compounds-CT-DNA mixture was incubated for 10 mins before measuring the absorbance using UV-vis absorption spectroscopy [43]. An equal amount of CT-DNA was also added to the reference solution to get rid of CT-DNA absorbance.

The compounds intrinsic binding constant, K_b were determined using Wolfe-Shimer equation as follows:

$$\frac{[DNA]}{\varepsilon_a - \varepsilon_f} = \frac{[DNA]}{\varepsilon_b - \varepsilon_f} = \frac{1}{\varepsilon_b - \varepsilon_f} \quad (3)$$

Where [DNA], ε_a, ε_b, and ε_f are DNA concentration, apparent, fully bound complex, and free complex extinction coefficients, respectively. The ratio of the slope to the intercept from the plot of [DNA]/(ε_a - ε_f) against [DNA] gave the binding constant K_b of the compounds.

2.7.2 *Luminescence competitive displacement study*

A competitive displacement study was carried out using fluorescence spectroscopy between CT-DNA pre-treated with ethidium bromide (EB) and complexes **1–15** to establish the complexes' actual mode of binding to CT-DNA. Ethidium bromide in buffer solution has low fluorescence intensity due to fluorescence quenching of the free ethidium bromide by the solvent molecule, but on binding through intercalation to DNA, its emission intensity is drastically enhanced [44]. The competitive luminescence displacement assay was done using

prepared in a phosphate buffer of pH 7.2 and left to equilibrate for 30 mins. Keeping CT-DNA-EB concentrations constant, different concentrations (0-20 µM) of the complexes were added at 8 mins interval for equilibration at room temperature. The fluorescence quenching ability of CT-DNA bound EB by the complexes were recorded in the wavelength range of 530-700 nm with an excitation wavelength at 525 nm at 25 °C.

$$\frac{F_o}{F} = 1 + K_{SV}[Q] = 1 + K_q\tau_o[Q] \quad (4)$$

A Stern-Volmer equation 4, was used to evaluate the CT-DNA-EB fluorescence quenching of the complexes. Where F_o and F denote the relative fluorescence intensities of CT-DNA in the absence and presence of the quencher, $K_{sv,}$ Stern-Volmer quenching constant, [Q], quencher concentration, Kq, bimolecular quenching constant and τ_o, average lifetime of the fluorophore in the absence of the quencher which is typically equal to 10^{-8} s in biomacromolecules.

2.7.3 *Albumin binding assay using absorption spectroscopy titration*

Absorbance assay of albumin binding is a very simple method used in identifying the conformational changes in protein. A stock solution of bovine serum albumin (BSA) was prepared by dissolving an appropriate amount of BSA in phosphate buffer saline solution (pH 7.2) under constant stirring for 1 h at 25 °C. It was kept at 4 °C and used within four days. The BSA concentration was determined spectrophotometrically by using ε280 = 44300 M^{-1} cm^{-1} absorption coefficient. The stock solution of the complex was prepared by dissolving 1 mmol of the complexes in DMSO. Absorption titration assay was done by adding different concentrations (0–10 µM) of the complexes to a constant BSA concentration (6 µM). The samples solution was incubated after each addition of the concentrations for 10 mins at 25 °C before recording the absorbance at λmax 280 nm. Binding constant K_b was calculated from the intercept to the slope ratio of 1/[A - A°] vs. 1/[complex] linear curve where A and A° represent BSA absorbance in the presence and absence of complexes, respectively [46].

2.7.4 *Albumin binding studies using fluorescence quenching method*

A solution of 1 µM of BSA was titrated against various concentrations of the complexes (0–35 µM) and incubated for 8 mins at 25 °C. BSA was excited at 280 nm and emitted at 346 nm wavelength [22]. K_{sv} constant was determined from the Stern-Volmer equation:

$$I_o/I = 1 + Kq\,\tau_o\,[Q] = 1 + Ksv[Q] \quad (5)$$

Where I_0 and I represent the intensities of the fluorescence in the presence and absence of the quencher respectively while K_q, K_{sv}, τ_o, [Q] represent the BSA quenching rate constant, dynamic quenching constant, the average lifetime of BSA without the quencher ($\tau_o = 10^{-8}$ s) and concentration of quencher respectively.

3.0 Results and Discussion

3.1 *Synthesis and Characterization of L1 – L5*

L1 - L5 were prepared by the condensation reaction of 2-pyridine carboxaldehyde with five substituted anilines (2-aminophenol, **L1**; 2-aminobenzenethiol, **L2**; 2-fluoroaniline, **L3**; p-toluidine, **L4**; and 2-thiophenemethylamine, **L5**) in anhydrous ethanol, all in excellent yields. The reactions were monitored using IR and were further characterized using ^{1}H NMR, ^{13}C NMR, mass spectrometry, UV-Vis, and melting points. In the IR spectra of ligands **L1**–**L5**, the absence of carbonyl stretching bands and appearance of the imine ν(C=N) absorption band between 1620 and 1625 cm^{-1}, revealed the successful synthesis of the proposed Schiff base ligands. ^{1}H NMR spectra of **L1**, **L3**, **L4,** and **L5** in deuterated acetone exhibited singlets at 8.81, 8.65, 8.59 and 8.44 ppm respectively attributed to the azomethine (CH=N) proton. There was no azomethine proton resonance in the spectrum of **L2** due to cyclization of the ligand through S atom to form 2-(pyridin-2-yl)benzo[d]thiazole. All the physical and spectral data for the known ligands [23-28] were in agreement with the ones previously reported.

3.2 *Synthesis and characterization of the complexes*

Complexes **1 - 15** were synthesized by reacting two equivalents of the respective ligands with one equivalent of the silver(I) salts in anhydrous ethanol. The complexes were obtained in good to excellent yields of between 60 and 97 % as air-stable solids. The formation and purity of the products were confirmed by various spectroscopic and analytical techniques. The scheme below represents the synthesis route for complexes **1** to **15**.

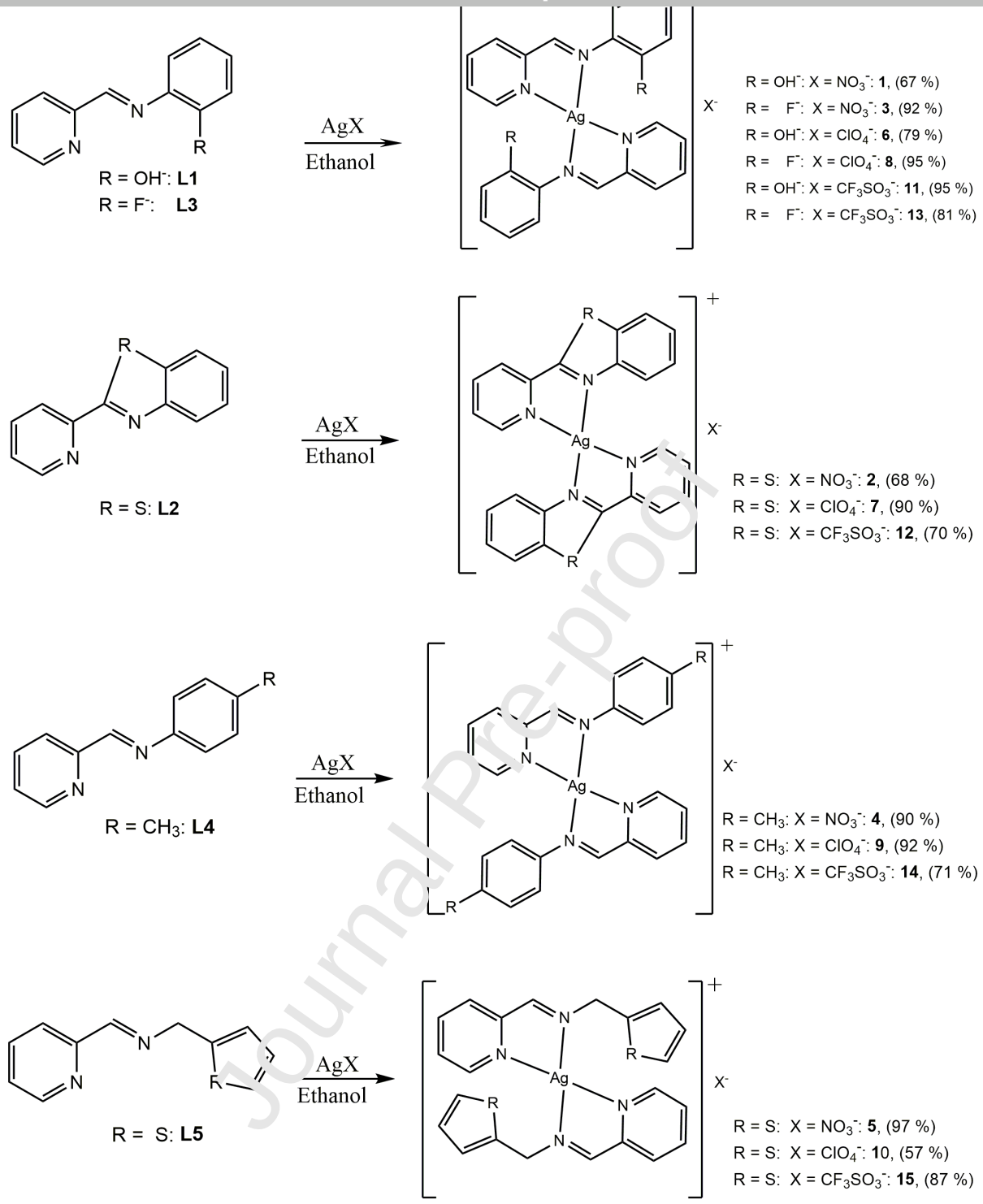

Scheme 1: Synthesis of complexes **1** – **15** under constant magnetic stirring in anhydrous ethanol

Coordination of **L1**–**L5** to the Ag(I) centers were monitored by comparing the FT-IR spectrum of the free ligands to their respective complexes (see supplementary info **Table S1**). The Bands at 1620–1622 cm^{-1} in the FTIR spectra of **L3** and **L4** ligands associated with the -C=N- bond stretching frequencies shifted to higher frequencies between 1625 and 1628 cm^{-1} band upon coordination to Ag(I), while in the spectra of **L1** and **L5** bands shifted to lower

coordination. In the spectrum of **L2** with thiazole moiety, the -C=N- bond shifted from 1457 cm^{-1} to higher frequency in the spectra of **2**, **7** and **12** between *ca.* 1461–1490 cm^{-1}. The absorption bands associated with the pyridinyl ring in the range 1579–1585 cm^{-1} in the spectra of **L1**–**L5** shifted to 1583–1593 cm^{-1}. Coordination of **L1, L3, L4,** and **L5** to Ag(I) was via N_{im} and N_{py} donor atoms, while for **L2** coordination was via $N_{thiazole}$ and N_{py} donor atoms, similar to reports of related structures in literature [47]. Bands attributed to anionic functional groups were observed in all the complexes with strong sharp bands attributed to NO_3^-, $\nu 3$ asymmetric stretch for ClO_4^-, and SO_3^- of the triflate anion, observed between 1273 and 1335 cm^{-1} in the spectra of **1–5**, 1067 and 1096 cm^{-1} in the spectra of **6–10**, and at 1025–1026 cm^{-1} in the spectra of **11–15** respectively.

The ^{1}H-NMR spectra of protons close to the donor atoms in **L1**–**L5** were compared to **1–15** ^{1}H-NMR spectra (see supplementary info **Table S1**), and a noticeable downfield shift in the protons around N atoms was observed. In the spectra of complexes with **L1, L3, L4,** and **L5** as the ligands, the azomethine alpha protons and for those with **L2** as the ligand, the thiazole -C=N- alpha protons with respect to their pyridinyl N, shifted downfield relative to those of their respective free ligand. This is an indication of coordination of the Ag(I) center via the imine N and pyridinyl N atoms in the complexes of **L1, L3, L4,** and **L5**, and to the thiazole N and pyridinyl N atoms in the complexes of **L2**.

The mass spectra of **1–15** in acetonitrile or methanol were all obtained in the positive ion mode and are a confirmation of coordination to Ag(I) centers in all complexes. The spectra all showed signals, which correspond to species containing the ligands together with the silver ion and sometimes in the presence of solvent molecules. There were peaks at 503 for complexes **1, 6** and **11** arising from $[Ag(L1)_2]^+$, 533 for **2, 7** and **12** corresponding to $[Ag(L2)_2]^+$ while for **3, 8** and **13** and **4**, **9** and **14** at m/z 509 and at m/z 501 corresponding to $[Ag(L3)_2]^+$ and $[Ag(L4)_2]^+$ respectively. For complexes **5, 10** and **15**, the molecular ion peak at m/z 513 corresponded to $[Ag(L5)_2]^+$.

Complexes **1** – **15** are soluble in most polar solvents, some in water as well. Their molar conductivities measured in dimethylformamide at 25 °C gave values which range between 1.02 and 3.48 x 10^4 S m^{-2} mol^{-1} (see supplementary info Table S2), indicating that the complexes act as electrolytes. The electronic behaviours of **L1** – **L5** and **1** – **15** were studied using UV-vis spectrophotometry with the spectra recorded in acetonitrile. **L1** and **L4** show absorption bands each at 289 and 289 nm, and 362 and 329 nm respectively attributable to π–π* and n–π* transitions. **L2, L3,** and **L5** each have one absorption band at 309, 284, and 238

band, while **6** and **11** have two absorption bands, similar to those of **L1**. The two bands in the spectra of **6** and **11** were observed at 323 and 359 nm, 289 and 293 nm, respectively. It is possible that in the spectrum of **1**, the two overlay and are observed in the broad band at 334 nm. These bands attributed to intra-ligand n–π* and π–π*, as well as metal to ligand charge transfer transitions (MLCT) since no *d–d* transitions are expected for d^{10} silver(I) complexes [51, 52]. There is generally a slight red-shift in the spectra of all complexes relative to those of ligands associated with a decrease in energy at the excited states upon coordination to silver(I) [53-55]. The absorption patterns of complexes **4, 6, 8, 9, 11,** and **14** are similar having two absorption bands at 321–359 nm, which may be attributed to the n–π* transition and 290 – 308 nm allied to π–π* transition in the ligand. Generally, the presence of different phenyl substituents ranging from electron-donating to electron-withdrawing as well as different counter ions bring about the different electronics properties of complexes 1-15. Sterically, the complexes differ slightly due to the great resemblance in the backbone of L1-L5 and this agrees with their similar Ag(I) complexes spatial geometry structures. Although, the influence of steric effect of the substituents or the counter ion can be observed from the discrepancies in the complexes N–Ag–N bond lengths and angles. However, the electronic effect, steric effect and the nature of the counter ion have less influence on the shape of complexes 1-15.

3.3. Crystal structures of complexes 4, 5, 8, 9 and 15

The *ORTEP* diagrams, along with the atom numbering schemes for complexes **4**, **5**, **8**, **9**, and **15** are shown in Fig. 1**.** Firstly, all complexes feature two sets of planes. In the first set of planes, Plane 1 can be described by a five-member metallacycle including the pyridine imine unit and Plane 2 is described by substituted phenyl ring for **4**, **8** and **9**. In all complexes, two ligands coordinate to the metal center thereby resulting in a pseudo-tetrahedral geometry. In this communication, the dihedral angle between the two planes formed by the metallacycles is defined as *θ*. Only **4**, **8** and **9** posses plane 2. The dihedral angles between plane 1 and plane 2 described above are hereby denoted γ. The second set of planes are in the structures of complexes **5** and **15** and are defined by the thiophene ring along with the methylene linker. In the asymmetric unit of complex **4**, are two molecules of the cation $[Ag(L4)_2]^+$ and two molecules of the NO_3^- anion. The two cationic molecules are not related by symmetry and display differences in the conformations of the L4 moieties wherein molecule 1, the angle γ seems to be smaller in molecule 2 (1.41(7) and 9.73(8)°) compared to molecule 1 (24.15(9)

with no dihedral γ angle as Planes 1 and 2 are linked via a CH_2 linker. **8** has ½ a molecule of the cation $[Ag(L3)]^+$ and ½ a molecule of the perchlorate anion with a γ angle of 38.62(7)°. In the asymmetric unit of **9** are one and a half molecules of the cation $[Ag(L4)_2]^+$ and $[Ag(L4)]^+$ and similarly one and a half molecules of the perchlorate anions. In the structure of the full molecule, the γ angles are different for each set of planes of each ligand coordinated to the Ag(I) center and whereas one displays near coplanarity (6.77(6)°), the other has a dihedral angle of 25.23(4)°, and 24.63(4)° in the half molecule. The asymmetric unit of **15** has half a molecule of the cation $[Ag(L5)]^+$, one molecule of the anion $CF_3SO_3^-$, and a molecule of water. This fashion of coordination and arrangement in the asymmetric units is similar to those reported by our group [29].

Secondly, in all complexes, the metal centre coordinates to two ligands *via* the pyridine N and the imine N atoms in a bidentate manner with the anion outside the coordination sphere. Since the geometry around the metal centre is pseudo-tetrahedral in each case, the dihedral angles between the chelate rings involving the metal center, defined by θ in this communication, in each complex vary but ranges between 64.16(4) in complex **9** and 88.99(7)° in complex **5** (see supplementary info Table S3). The angles around the Ag(I) centres are either acute and range between 71.83(10) and 73.14(5)°for the chelate ring moieties or obtuse and range between 109.53(5) and 153.09(6)°. The obtuse N_{py}−Ag−N_{im} angles of the complexes **4, 5, 8, 9** and **15** range between 113.44(9) and 135.72(10)° (see supplementary info Table S4) showing their deviation from an ideal tetrahedral geometry. Geometry index for four coordinates complex τ_4 (equation 6) was used to determine the complexes geometry

$$\tau_4 = \frac{360\,^\circ - (\alpha + \beta)}{141\,^\circ} \qquad \text{Equation (6)}$$

and the τ_4 values of the complexes fall within 0.52 – 0.67, which fits in Yang *et al.* [56] seesaw geometry description. Complexes **4, 5, 8, 9, and 15** are unsymmetrical structurally and, therefore, belong to the C_1 point group.

The Ag-N_{im} bond distances in **5** and **15** are generally shorter than the Ag—N_{py} bond distance but longer in **4, 8,** and **9,** but all fall within the expected range for Ag—N bond distances in literature for related compounds [47, 57].

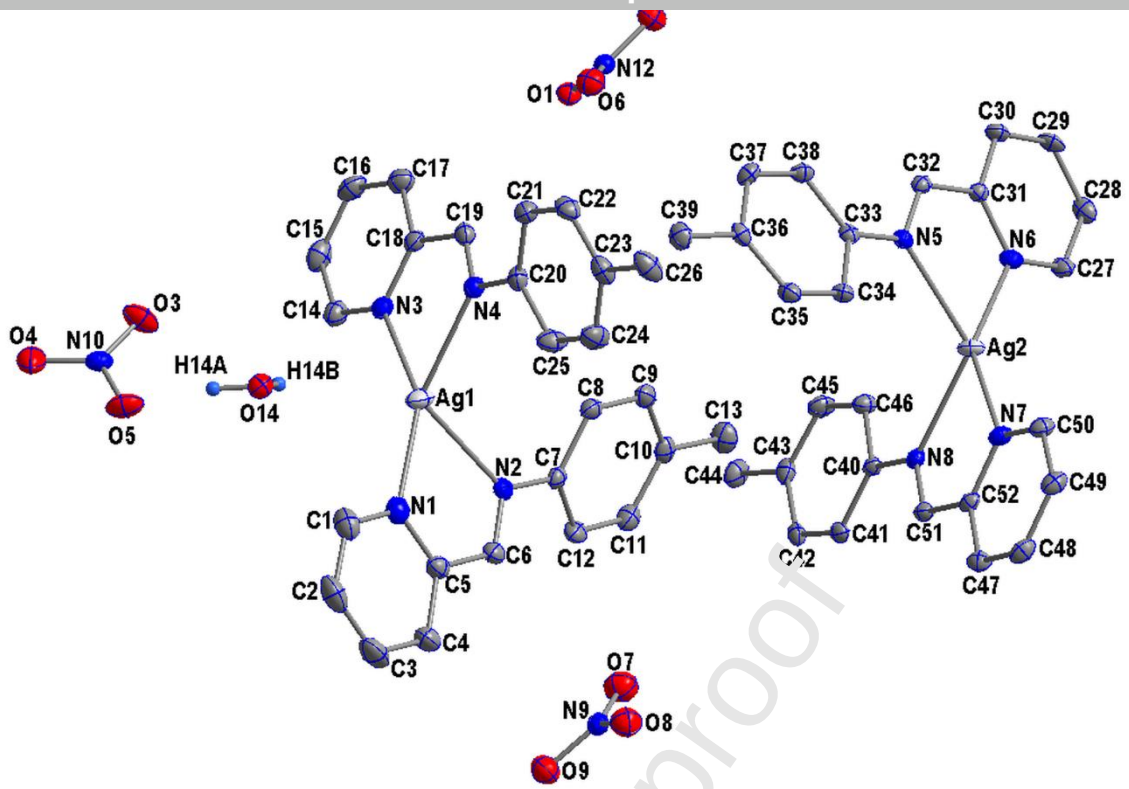

(a) 4

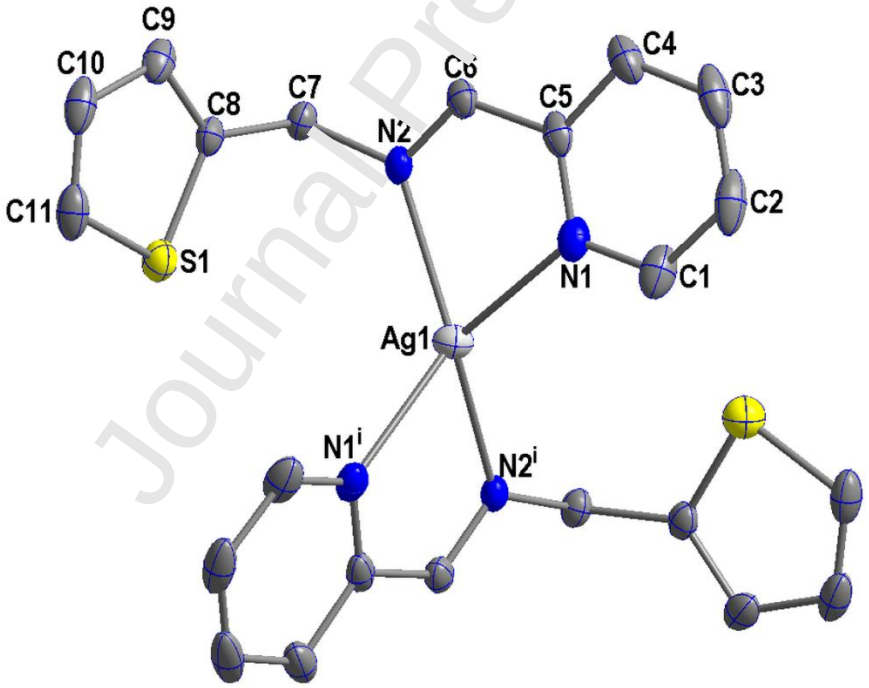

(b) 5

Journal Pre-proof

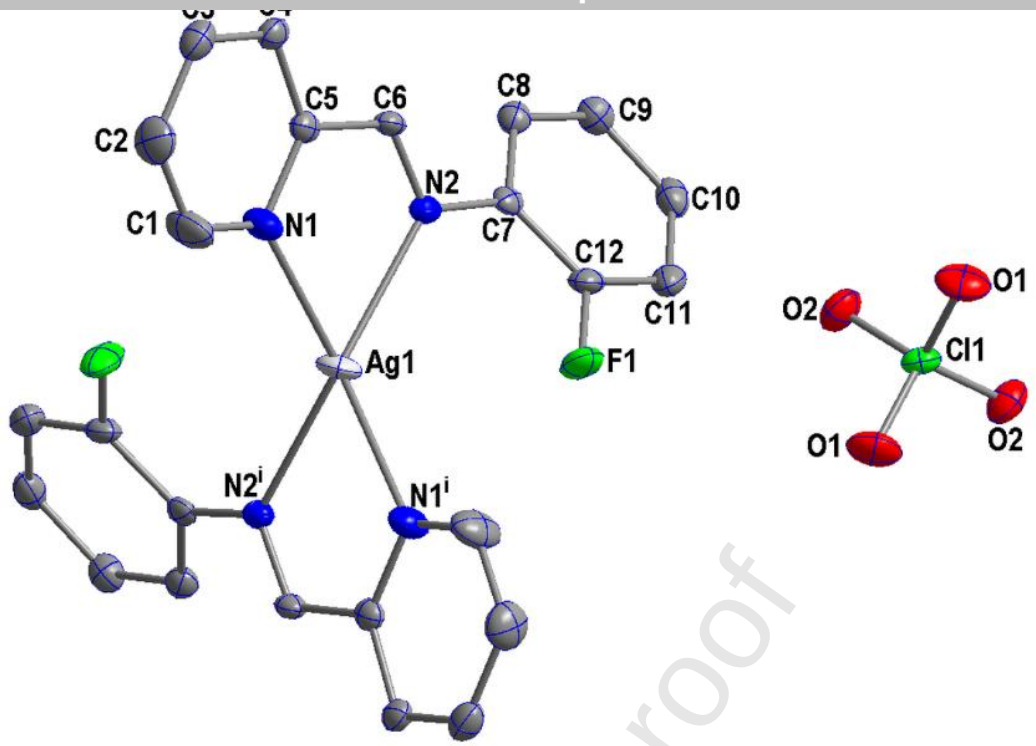

(c) 8

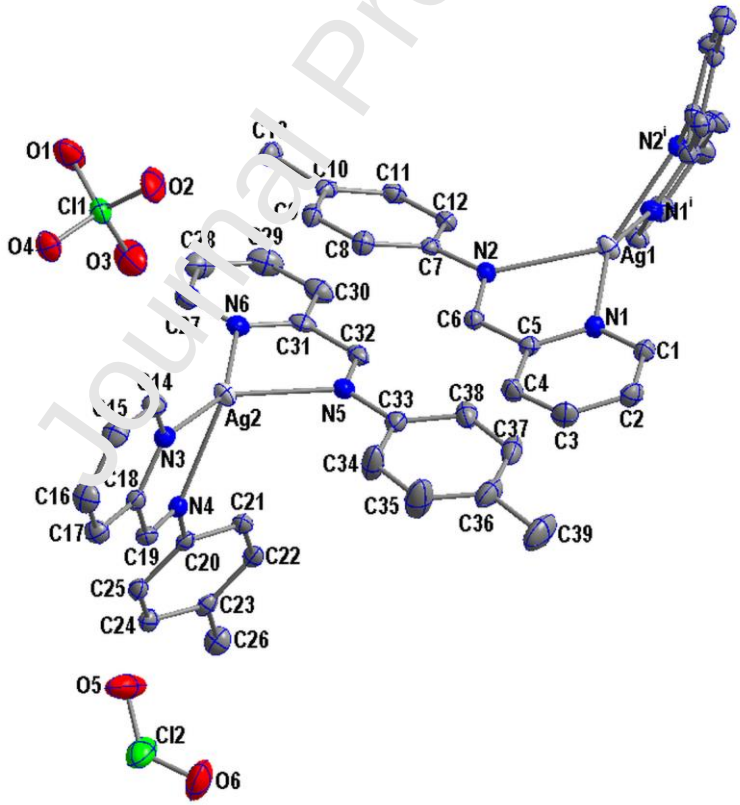

(d) 9

Journal Pre-proof

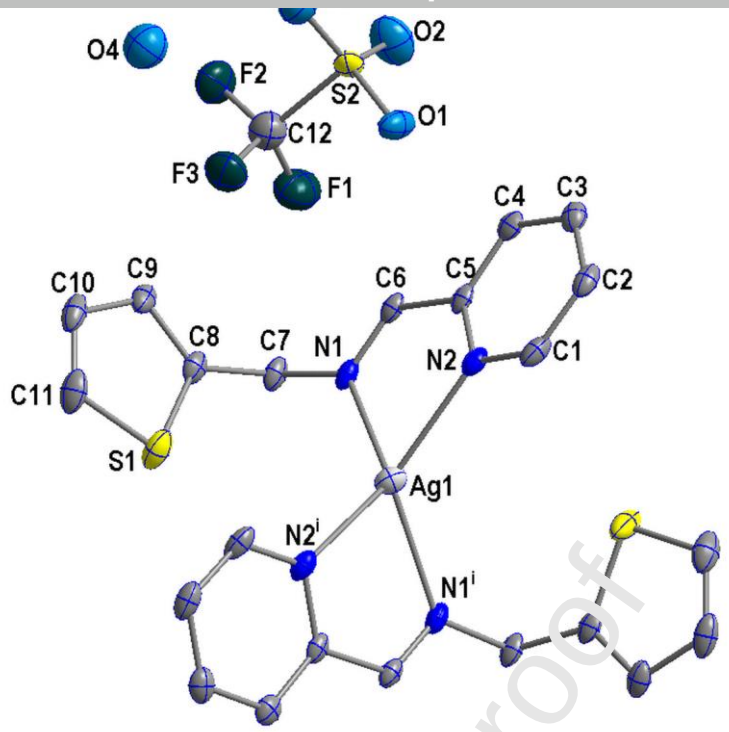

(e) 15

Figure 1: The ORTEP diagrams showing the atom numbering scheme with the thermal ellipsoids drawn at the 50% probability level for molecules of (a) complex **4**, (b) **5**, (c) **8**, (d) **9** and (e) **15**. Hydrogen atoms have been omitted for clarity except for the water molecule in **4**. Symmetry operators: Complex **5**, (i) = ½ - x, y, -z; Complex **8**, (i) = 2 - x, y, 2 – z; Complex **9**, (i) = -x, y, 3/2 - z and Complex 1**5**, (i) = 2 - x, y, ½ - z.

3.4 Biological Application Studies

3.4.1 *In-vitro* antimicrobial studies

L1 – L5 and **1 – 15,** along with ciprofloxacin (used as a standard), were screened for antimicrobial activity against two Gram-positive bacteria, MRSA and *S. aureus*, and four Gram-negative bacteria, *E. coli*, *S. typhi*, *K. pneumoniae*, and *P. aeruginosa*. **L1 – L5** were screened mainly to establish the contribution of the ligands biologically. The minimum inhibitory concentrations (MIC) given in Table 2 indicated that complexes **1 – 15** generally had better antibacterial activity compared to **L1 – L5**, an indication that complexation to Ag(I) enhanced the antimicrobial properties of **L1 – L5**. The complexes probably have a better ability to penetrate the bacterial cell membranes due to enhanced lipophilicity of the complexes. In such a process, the lipid layer of the microbe cells gets infiltrated, and the respiration process gets destroyed, thereby stopping bacterial growth [58]. There is a reduction in metal ion polarity on chelation to the ligand due to overlapping of the ligand orbital and partial sharing of the positive charge of the metal ion with donor groups. Also, the

subsequently aids permeation through the lipid layer of the cell membrane [59]. Amongst the ligands, **L1** and **L5** were the least active ligands with **L1** only active against *S. aureus*. **L5** had MIC values above 1000 µg/mL against all except against *E. coli* for which it was inactive. **L2** is selectively active against *S. aureus* and *P. aeruginosa*, **L3** against *E. coli*, *K. pneumoniae* and *P. aeruginosa* and **L4** against the notorious MRSA with activity similar to that of the standard ciprofloxacin.

The compounds were generally more active against *E. coli*, *S. typhi*, *K. pneumoniae*, and *P. aeruginosa.* Gram-negative bacteria often have a thinner cell membrane making accessibility easier. Complexes **5**, **6** and **10** showed the highest antimicrobial activity against all bacteria tested. The ligands of each of **5**, **6** and **10,** possess either the thiophene moiety or the hydroxyl substituent. Significant antimicrobial activity of compounds containing either thiophene moiety or hydroxyl substituent has been reported [27, 28, 60]. The high lipophilic nature of the thiophene moiety [61] in **5** and **10** which in turn influence membrane penetration is assumed to be responsible for their high activities. In **6**, the o-position of the hydroxyl substituent in phenyl ring could have limited its activity [62] as observed in **1** and **11** because the electron donating group and o-position of a substituent would lead to low lipophilicity but the presence of perchlorate anion in **6** must have enhanced the activity. Therefore, the counter anions could possibly also be aiding in lipophilicity [63].

In terms of selectivity, **8** and **10**, both with the 2-fluorophenyl and thiophen-2-ylmethyl moieties were more active against *S. aureus* each with a value of 0.8 µg/mL MIC. **3**, **5** and **7** which have MIC values between 0.025 – 0.4 µg/mL, were active against MRSA.

The metal salts on their own seem to be fairly active. On complexation, only complexes **8** and **10** seemed to show MICs lower (0.8 µg/mL) than those of $AgNO_3$ and $AgClO_4$ (3.125 µg/mL) against *S. aureus*. **L3** is inactive while **L5** is least active but when complexed to $AgClO_4$, the activity increases as observed for complexes **8** and **10** with F and S atoms in the structures of the ligands. Only **7** had a lower MIC (0.1 µg/mL) than the salts and the standard against MRSA. It is assumed that the ClO_4^- anion and the presence of S moiety could probably have a contribution to the lower MIC value. Complexes **7, 9,** and **10** are fairly active, with their MIC values the same as their metal salt against *E. coli*. The enhanced activity of **4** with Methyl substituent is almost 4 times and for complex **3**, 1000-fold. The activity of **4** was similar to that of the standard, while that of **3** was much better than that of the standard, both with the F^- substituent. The activities of **6** (with OH^-), **13** (with F^-), and **14** (with thiophene) against *S. typhi* are the same as the standard. Complex **2** (with S moiety and NO_3^- as the anion), the MIC value was half that of the standard but similar to that of $AgClO_4$

values (0.05 µg/mL) than the standard, while **10** with the thiophene moiety had a MIC value same as that of the standard against *P. aeruginosa* (**6, 9,** and **10,** all have ClO_4^- as the anion). In general, the substituents OH^-, F^-, thiazole and thiophene and the anion ClO_4^- seem to play a role when incorporated in the complexes leading to enhanced antimicrobial activities when compared to the ligands and or the salts against the different microbes. A comparison bar chart representing each salt complexes is shown in Fig. 2a, 2b and 2c. Compounds with 1000 µg/mL MIC value and those without antimicrobial activity are omitted from the bar plot for clarity.

Table 2: Minimum inhibitory concentration of silver complexes of L1-5 (µg/mL)

Compounds	Gram +ve Bacteria		Gram -ve Bacteria			
	SA	**MRSA**	**EC**	**ST**	**KP**	**PA**
L1	1000	NA	NA	NA	NA	NA
L2	12.50	NA	1000	NA	NA	6.25
L3	NA	1000	3.125	NA	25.00	3.125
L4	NA	25.00	1000	NA	1000	1000
L5	1000	1000	NA	1000	1000	1000
1	1000	12.50	1000	1000	6.25	12.50
2	12.50	12.50	1000	0.20	6.25	1000
3	25.00	0.40	0.0125	0.80	0.40	1000
4	12.50	50.00	0.20	1000	1000	6.25
5	12.50	0.025	12.50	1.60	0.80	12.50
6	12.50	12.50	6.25	0.40	0.20	0.05
7	1000	0.10	0.80	NA	1000	1000
8	0.80	12.50	1000	12.50	0.05	12.50
9	1000	12.50	0.80	0.80	1000	0.05
10	0.80	12.50	0.80	6.25	12.50	0.80
11	25.00	12.50	100	1000	1000	12.50
12	12.50	1000	0.80	50.00	0.40	1000
13	25.00	1000	25.00	0.40	12.50	12.50
14	1000	1000	50.00	0.40	3.125	1000
15	1000	1000	1000	1000	1000	1000
$AgNO_3$	3.125	0.20	12.50	1000	0.80	1000
$AgClO_4$	3.125	6.25	0.80	0.20	25.00	1.60
$AgCF_3SO_3$	NA	1000	1000	12.50	50.00	1000
Ciprofloxacin[s][37]	25.00	25.00	0.20	0.40	1.60	0.80

NA = No activity, s = standard, SA = *Salmonella typhimurium,* PA = *Pseudomonas aeruginosa*, EC = *Escherichia coli,* KP = *Klebsiella pneumoniae*, SA = *Staphylococcus aureus,* MRSA = methicillin-resistant *Staphylococcus aureus*

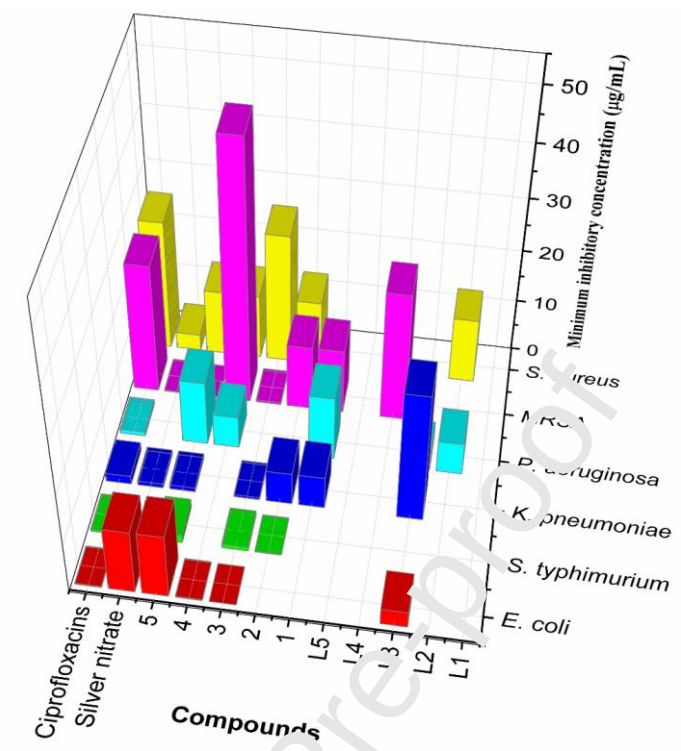

(a)

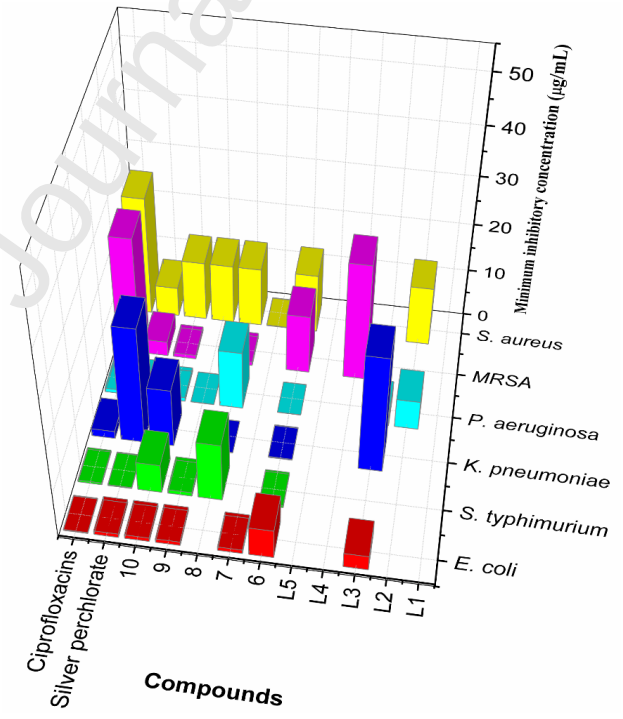

(b)

Journal Pre-proof

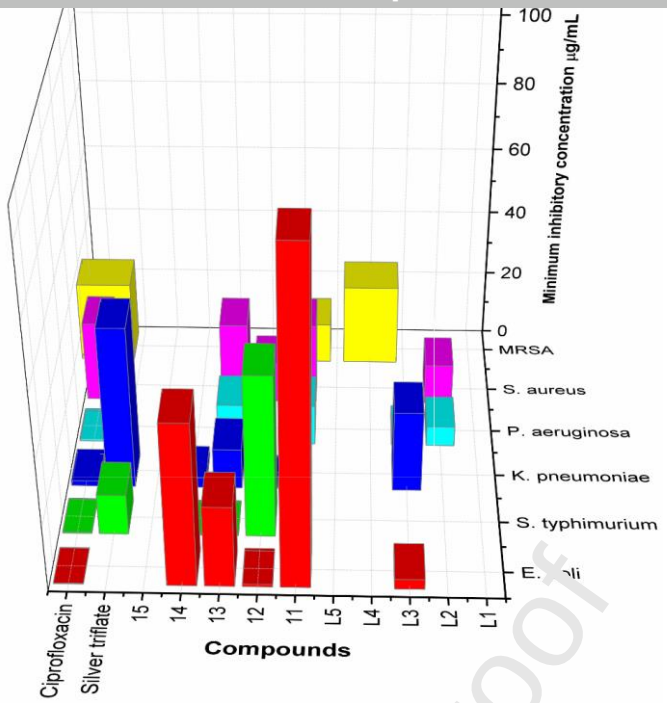

(c)

Figure 2: (a) Minimum inhibitory concentration (µg/mL) of **L1-L5** silver(I) complexes with nitrate as counter anion, (b) Minimum inhibitory concentration (µg/mL) of L1-L5 silver(I) complexes with perchlorate as counter anion and (c) Minimum inhibitory concentration (µg/mL) of **L1-L5** silver(I) complexes with triflate as counter anion.

3.4.2 *In vitro* antioxidant studies

Compounds with antioxidant activity such as dithiocarbamate complexes [37] and benzimidazole [64] have the abilities to slow down and stop damage to DNA, RNA, protein substrates and thereby prevent the occurrence of diseases such as cardiovascular disease, diabetes, rheumatism, atherosclerosis, cancer and aging [65]. Active antioxidant agents act as single electron transfer agents or as hydrogen atom transfer agents, and can also bind to transition metals [66]. The free radical scavenging ability of **L1 – L5** and **1 – 15** were studied using 2,2-diphenyl-1-picrylhydrazyl (DPPH) and ferric reducing antioxidant power (FRAP). In antioxidant studies, DPPH with absorbance at 517 nm, are frequently used in determining radical scavenging properties of the compounds. It is known to be a stable free radical with an odd electron in its structure that acts as an electron acceptor or a radical hydrogen acceptor to form a stable diamagnetic molecule. DPPH free radical scavenging method relies on its decolorization in the presence of an antioxidant agent, which leads to a decrease in its absorbance as the number of electrons accepted increases and can then be quantitatively evaluated [67] in comparison to a standard. The ferric reducing antioxidant power (FRAP) assay is often preferred because it is simple, fast, economical, and direct in antioxidant

compound. This involves the reduction of a colourless Fe^{3+} tripyridyltriazine complex (Fe^{3+}(TPTZ)) to an intense blue-coloured Fe^{2+} tripyridyltriazine complex (Fe^{2+}(TPTZ)) by the electron-donating antioxidants at low pH [68].

Table 3 summarizes the mean values from three independent experiments of in vitro antioxidant activities of **L1 – L5** and Complexes **1 – 15** at different concentrations. The antioxidant activities of the compounds are expressed as 50 % inhibitory concentration (IC_{50} in mg/mL). Ascorbic acid with an IC_{50} value of 1.0 x 10^{-3} mg/mL and 2.68 mg/mL was used as a standard for DPPH and FRAP studies, respectively. The standard ascorbic acid value for DPPH is comparable to those of Borra *et al.* [69] and Saravanakumar *et al.* [70].

Table 3: Mean ± standard deviation values of In vitro antioxidant activities of **L1 – L5** and Complexes **1 – 15** from three independent experiments.

	Antioxidant(IC_{50} mg/mL)	
COMP.	DPPH	FRAP
1	8.32 x 10^{-1} ± 0.002	6.14 x 10^{-5} ± 0.0005
2	1.71 x 10^{-2} ± 0.005	1.1939 ± 0.0094
3	3 x 10^{-2} ± 0.007	1.52 x 10^{-1} ± 0.002
4	11.732 ± 0.28	3.96 ± 0.023
5	9.2 x 10^{-2} ± 0.014	2.64 x 10^{-2} ± 0.005
6	6.79 x 10^{-1} ± 0.003	7.01x 10^{-16} ± 0.00
7	1.33 x 10^{-1} ± 0.017	2.086 ± 0.067
8	2.803 ± 0.029	8.774 ± 0.78
9	NA	1,18 ± 0.0088
10	4.3 x 10^{-2} ± 0.002	26.2762 ± 3.34
11	6.1 x 10^{-2} ± 0.008	33.1538 ± 4.48
12	7637.256 ± 625.26	6.44 ± 0.050
13	306.651 ± 16.59	4.14 ± 3.90
14	NA	1.66 ± 0.037
15	0.654 ± 0.003	1 x 10^{-4} ± 0.0004
L1	NA	63.86 ± 9.97
L2	3.81 ± 0.05	18.084 ± 2.07
L3	NA	4.3 x 10^{-1} ± 0.017
L4	71.607 ± 2.93	NA
L5	82.16 ± 3.23	NA
As	1 x 10^{-3} ± 0.0004	2.67562 ± 0.11

NA = Not Active, As = Ascorbic Acid

Complexes **1** – **15** were assayed for free radical scavenging activity by DPPH and FRAP method and are presented graphically as Fig. 3a and 3b, respectively. The IC_{50} values of **L1** –

values compared to their free ligands. Complexes **2**, **3**, **5**, **7**, **10** and **11** had good antioxidant activity between 0.017 – 0.133 mg/mL (Table 3). Compounds with benzo[d]thiazole moiety were the best scavengers with **2** having the highest amongst them. These are in agreement with antioxidant activity of structurally related compounds [71, 72]. The S atom acts as a donor of an electron which stabilizes the free radicals. Similarly, complexes **5** and **10** showed high activities, probably due to the lone pair of electrons on their thiophene moieties. Similar activities have been reported with thiophene containing compounds [73]. However, complexes **12** and **13** had the lowest activities with 306.65 and 7637.26 mg/mL IC_{50} despite **12** having S on the thiazole moiety. Both complexes have triflate anion, which may be the reason for the poor effects on the activity of the compounds. Complexes with p-tolyl substituent generally had low antioxidant activity and even no activity at all, as observed for **4, 9,** and **14.** Significant antioxidant activities were observed in FRAP for complexes **1, 2, 3, 5, 6, 7, 9, 14** and **15.** Most of the complexes showed higher activity than ascorbic acid, whose IC_{50} value is 2.68 mg/mL. This implies that the complexes' ability to reduce Fe^{3+} to Fe^{2+} was good. Complex **6,** in particular, with an IC_{50} value of 7.01 x 10^{-16} mg/mL, had the lowest ferric reducing power attributable to the hydroxyl group in the compound. This kind of activity has been observed for compounds of phenolic nature [41].

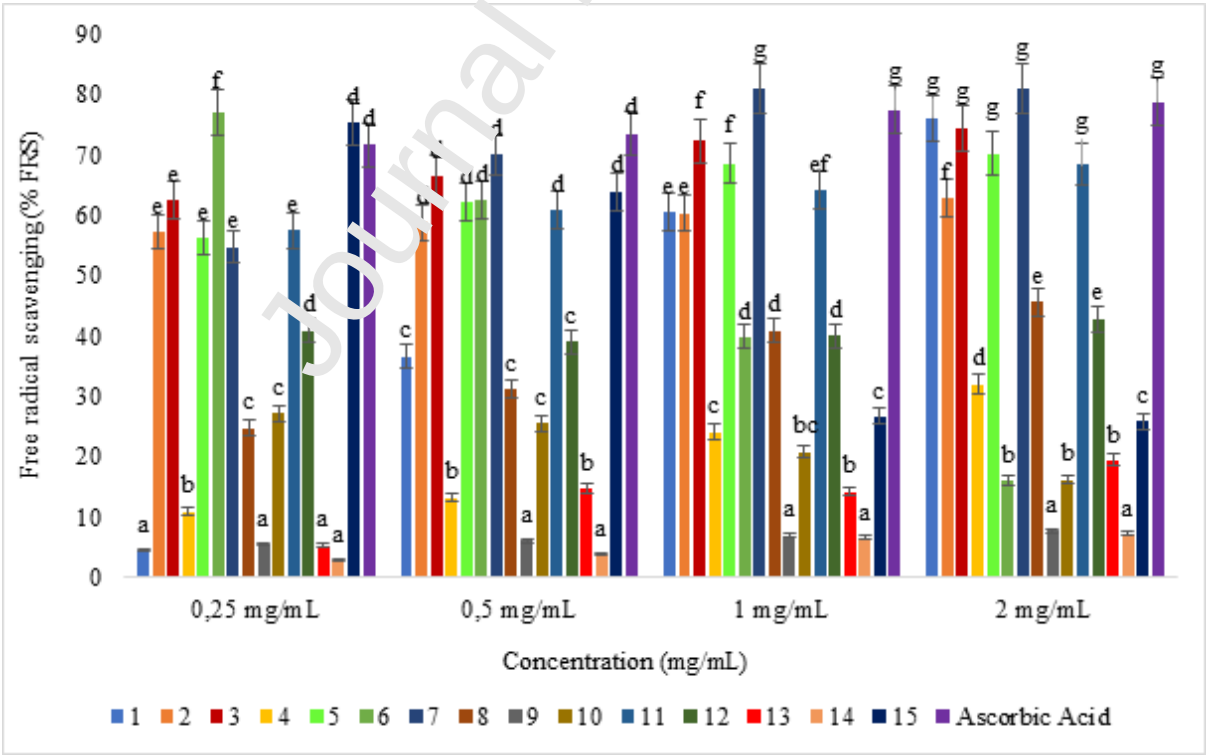

Figure 3a: DPPH % free radical scavenging vs. concentration (mg/mL) of complexes 1–15 and Ascorbic Acid. Values represent mean ±standard deviation (n = 3). [a-g]Different alphabets over the bars

range post hoc test, p<0.05).

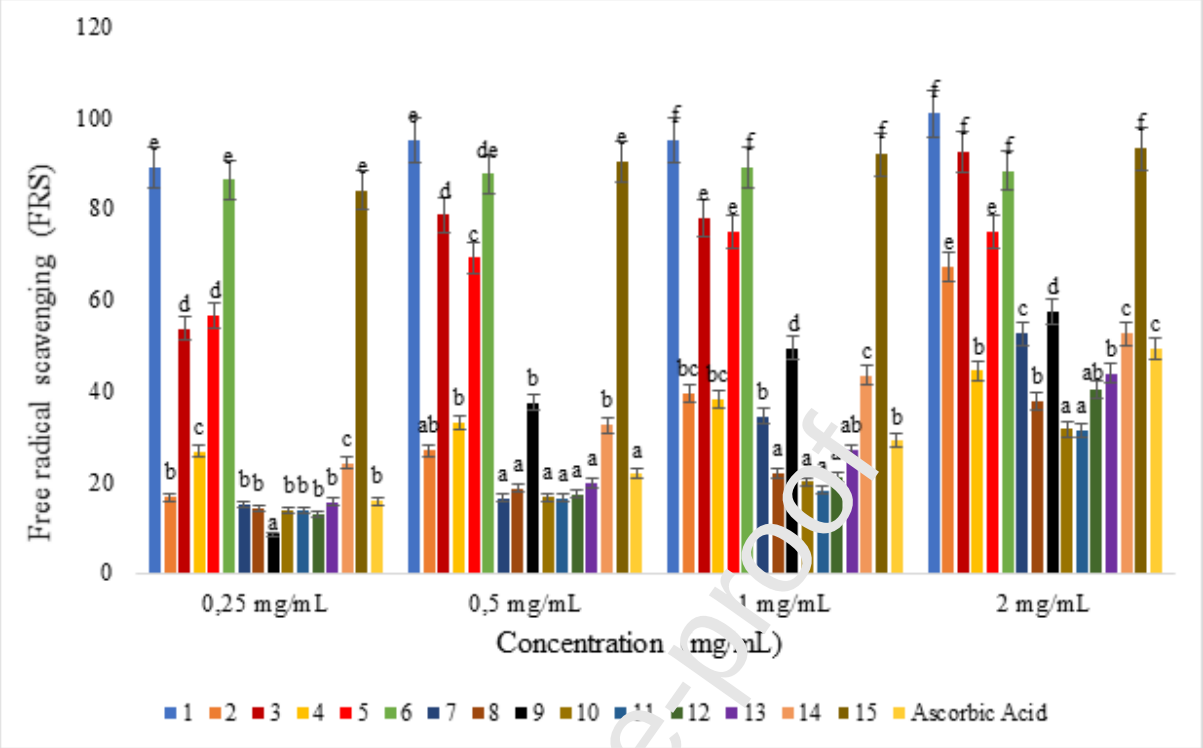

Figure 3b: FRAP % free radical scavenging vs. Concentration (mg/mL) of complexes **1**–**15** and Ascorbic Acid values represent mean ±standard deviation (n = 3). [a-f]Different alphabets over the bars for a given concentration for each complex represent significant difference (Turkey's-HSD multiple range post hoc test, p<0.05).

3.4.3 *DNA binding studies*

Metal complexes are known to bind to DNA either *via a* covalent or a non-covalent bond. When binding is *via* a covalent bond, the basic DNA N atom is replaced by the metal complex's labile ligand while in the case of binding through non-covalent bonds, the metal complex - DNA helix involves, intercalation, electrostatic or groove binding along the major or minor grooves of the DNA [74]. We are interested in Ag(I) for two reasons; at low concentrations, it is non-toxic to the human body and secondly, Ag ions interact with DNA in such a way that it can cause disturbance to the functionality of nucleic acids [18, 39, 75].

In this research we set to examine the extent to which **L1 – L5** and **1 – 15** interacts by electronic absorption titration and by looking at hyperchromic and hypochromic effects on free calf thymus DNA (CT-DNA) and CT-DNA in the presence of **L1 – L5** and **1 – 15.** The absorption spectra showed prominent hypochromic shifts with absorption bands between 260 and 309 nm, with each increase in the CT-DNA concentration. This is an indication of intercalating binding behaviour to CT-DNA. Intercalators are molecules that stack

hydrogen bonds between DNA bases.

The absorption spectra of **L1 – L5** and **1 – 15** in the absence and presence of CT-DNA at a constant concentration of complexes are shown in Fig. S3-S21 (see supplementary info). Complexes **1 - 15** exhibited a prominent intraligand π□π* absorption bands between 260 and 309 nm. A hypochromic shift in the absorption bands with hypsochromic between 1-8 nm was observed in all the complexes (supplementary info Fig. S8-S21) except **2, 7, 10,** and **11,** whose absorption bands are accompanied by a slight bathochromic shift between 1-7 nm as the concentration of the CT-DNA was increased. The hypochromic effects of the absorption band can be attributed to intercalative binding mode which involves strong stacking interaction between the pyridinyl planar aromatic chromophore and the base pairs of CT-DNA [76].

The intrinsic binding constant of **L1 – L5** and **1** – **15** were evaluated from Wolfe-Shimer equation (Eq. 1) by determining the ratio of the slope to the intercept from the plot of [DNA]/(ε_a - ε_f) *versus* [DNA] (Fig. 4b). The binding constant obtained for **1 - 15** are between 1.5 x 10^5 and 3.5 x 10^6 M^{-1} while for **L1 - L5** they are between 5.00 x 10^4 and 1.38 x 10^5 (Table 4). The binding affinity of the ligands are lower than those of the complexes, an indication that the ligands binding affinity were enhanced on complexation to Ag(I). The complexes generally showed relatively moderate to high binding affinities. Complex **6** had the highest binding affinity (Fig. 4a) and **3** (Fig. S10) had the lowest affinity. Those of 9 (Fig. S15) and **15** (Fig. S21) are also high. It is not certain what the cause of these high affinities in complexes **6**, **9** and **15** but we suspect that π–π stacking has a major contribution to the affinities. The affinity of **6** is probably also complimented by interactions between the OH^- group and the DNA base [74]. This interaction favours the aromatic environment of the CT-DNA base pairs resulting in strong structural perturbations in the DNA molecule. These perturbations increase the distance between the adjacent base pairs [76]. Complex 6 high DNA interaction agrees with similar reported outstanding silver(I) imine complexes [43]. Generally, the observed trend in hypochromic shifts order is **6** > **9** = **15** > **11** > **5** > **4** > **8** = **14** > **13** > **10** = **12** > **1** > **2** > **3** = **7**.

Table 4: The binding parameters of Complexes **1-15** interactions with CT-DNA, ethidium bromide and bovine serum albumin

Cmp.	CT-DNA-Comp.	CT-DNA-EB -Complex	Protein -Complex

Journal Pre-proof

			(M^{-1}) x 10^4	($M^{-1}S^{-1}$) x 10^{12}	(M^{-1}) x 10^5		(M^{-1}) x 10^5	(M^{-1}) x 10^4	($M^{-1}S^{-1}$) x 10^{12}	(M^{-1}) x 10^4	
1	2.50 x 10^5	0.99	3.62	3.62	6.43	1.23	0.0246				
2	1.70 x 10^5	0.99	3.47	3.47	1.06	1.11	0.2030	4.25	4.25	1.33	0.88
3	1.50 x 10^5	0.99	3.42	3.42	8.92	1.28	2.0500	4.48	4.48	1.79	0.93
4	1.30 x 10^6	0.99	3.68	3.68	2.11	1.17	0.0421				
5	1.50 x 10^6	0.99	3.75	3.75	3.04	1.20	0.9960	7.19	7.19	1.21	0.83
6	3.50 x 10^6	0.99	4.61	4.61	6.96	1.25	0.0553				
7	1.50 x 10^5	0.99	3.26	3.26	3.00	1.22	0.4120	8.38	8.38	2.42	0.88
8	1.00 x 10^6	0.99	4.64	4.64	1.52	1.11	2.1700	3.22	3.22	0.000 462	0.59
9	2.00 x 10^6	0.99	3.20	3.20	2.56	1.20	0.5150				
10	3.00 x 10^5	0.99	2.96	2.96	3.66	1.24	0.6720	2.98	2.98	4.51	1.03
11	1.80 x 10^6	0.99	3.89	3.89	2.79	1.20	0.0660				
12	3.00 x 10^5	0.99	3.78	3.78	3.19	1.19	0.1610	6.93	6.93	1.11	0.84
13	3.50 x 10^5	0.99	3.94	3.94	1.65	1.13	1.6200	2.48	2.48	1.20	1.12
14	1.00 x 10^6	0.99	4.17	4.17	1.32	1.11	0.1580				
15	2.00 x 10^6	0.99	2.97	2.97	6.26	1.29	0.7310	1.44	1.44	1.05	0.96
L1	1.38 x 10^5	0.96									
L2	5.00 x 10^4	0.97									
L3	5.00 x 10^4	0.96									
L4	1.38 x 10^5	0.96									
L5	1.25 x 10^5	0.95									

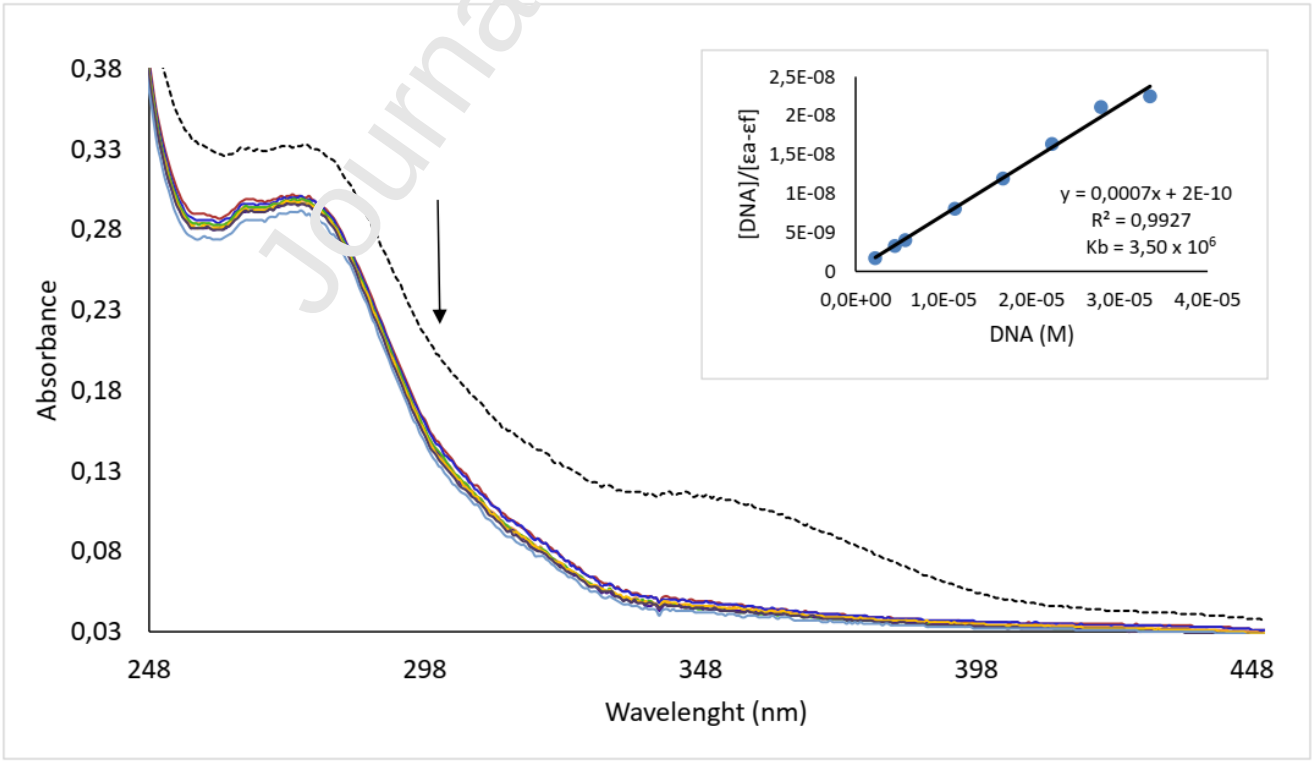

Journal Pre-proof

presence of different concentrations of CT-DNA (0 – 3.0 x 10^{-5} M) at 280nm λ_{max}. (inset) A stern-Volmer plot of **6** interaction with CT- DNA.

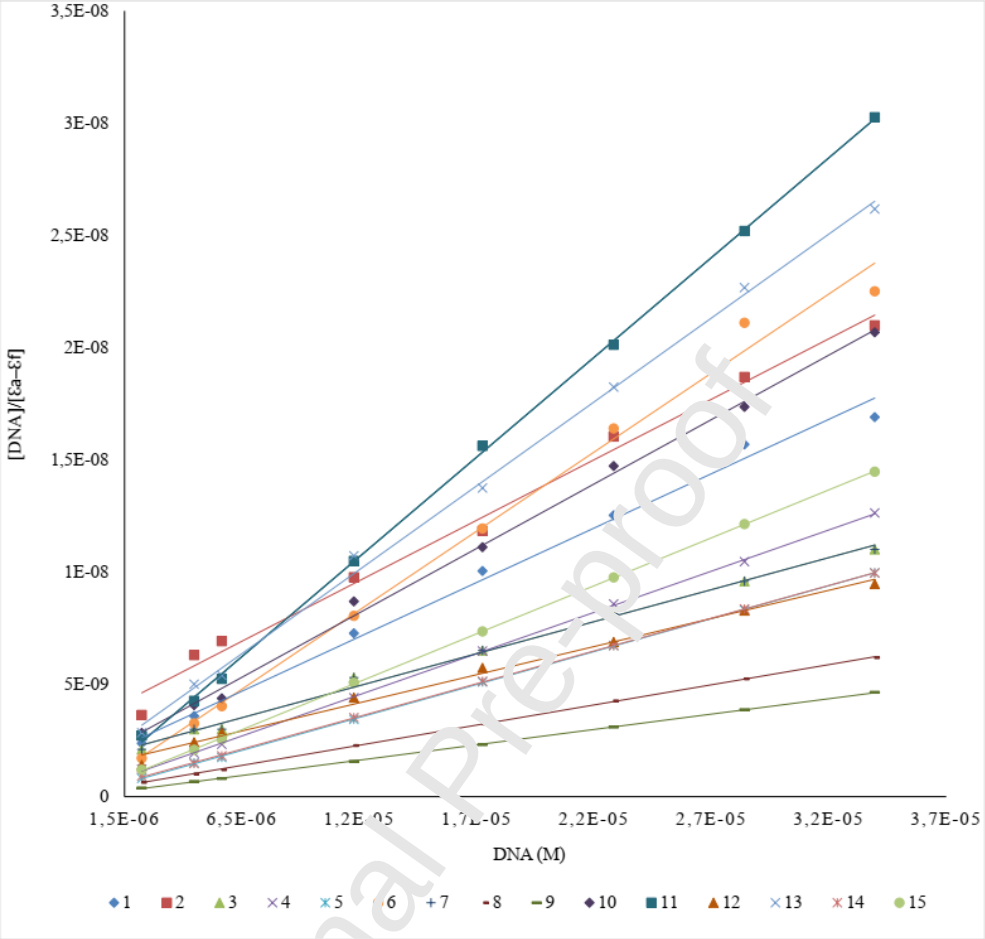

Figure 4b: The plot of [DNA]/(ε_a - ε_f) vs. [DNA] of complexes **1-15** interaction with CT- DNA.

3.4.2.1 *Luminescence competitive displacement studies*

A competitive binding study was carried out based on the displacement of ethidium bromide from the CT-DNA-EB adduct by the complexes, to determine 1 – **15** actual modes of binding to CT-DNA. Further studies of **L1 – L5** were exempted since their binding affinity to CT-DNA are lower than those of the complexes. Although the complexes absorb UV radiation, but they do not fluoresce.

EB is a known intercalating agent and also a strong emitter and is flat structurally, thereby sliding in between the DNA double helix base pairs [77]. The displacement of EB from EB-DNA adduct by another molecule would lead to the quenching of EB emission, which is an indication of an intercalation binding mode. The addition of increasing concentrations of **1 - 15** to a constant concentration of pre-treated CT-DNA-EB solution resulted in the decrease of

the slope to the intercept ratio of the linear quenching plot of F_o/F *versus* [complex]. The K_{sv} values for complexes **1 - 15** were between 2.96 and 5.50 x 10^4 M^{-1} (Table 4). These K_{sv} values indicated the displacement of EB by **1** to **15** and confirmed binding via intercalation mode to CT-DNA. The complexes have high quenching efficiency and a binding affinity to CT-DNA. Complex **8** (Fig. 5a) has the highest binding affinity to CT-DNA.

Fluorescence quenching is classified into two mechanisms, namely: static quenching and dynamic quenching. The static quenching involves the collision of the fluorophore and the quencher (complex) in the ground state while the dynamic quenching involves the collision of the fluorophore and the quencher in the excited state. In order to determine the type of quenching taking place, two approaches are commonly used namely: temperature-dependent approach and the linearity of the Stern-Volmer plot approach.

In this study, the linearity obtained in the Stern Volmer plots for **1 - 15** (Fig. 5b) indicated that the quenching fluorescence has only one mechanism, i.e., either dynamic or static. Evaluation of K_q using Equation **6** would suggest the quenching mechanism through which the complexes quench ethidium bromide emission.

$$K_{sv} = K_q \tau_o \tag{6}$$

Where K_{sv}, K_q, and τ_o represent Stern-Volmer quenching constant, bimolecular quenching constant, and an average lifetime of the fluorophore in the absence of the quencher, respectively. τ_o normally takes about 10^{-8} s in biomacromolecules [78]. The values of K_q obtained were between 2.96 and 5.50 x 10^{12} $M^{-1}S^{-1}$ (Table 4), which is greater than the maximum diffusion collision quenching rate constant of various quenchers of biological macromolecules (2×10^{10} $M^{-1}S^{-1}$) [78]. These results revealed that the quenching by 1 – **15** was not initiated by a dynamic mechanism but occurred via static quenching mechanism, thus at ground state, complexes formed between quenching molecules and fluorescence molecules are stabilized [79].

Another method of calculating binding constant of complexes **1 - 15** and CT-DNA can be by using the double-logarithmic Equation **7**

$$\log \frac{F_o - F}{F} = \log K_b + n \log[Q] \tag{7}$$

A plot of log F_o – F/F vs. log [Q] of complexes **1 – 15** gave a straight line with a slope of *n* and y-axis intercept of log K_b (Fig. S36-S49) (where F_o and F denote the relative fluorescence intensities of CT-DNA in the absence and presence of the quencher, respectively while [Q] is the concentration of the quencher, K_b is the binding constant and *n* is the number of binding

that all the complexes bind to one reactive site on the CT-DNA. The corresponding results are shown in Table 3. Complex **3** (Fig. 5c) showed the most binding affinity to CT-DNA.

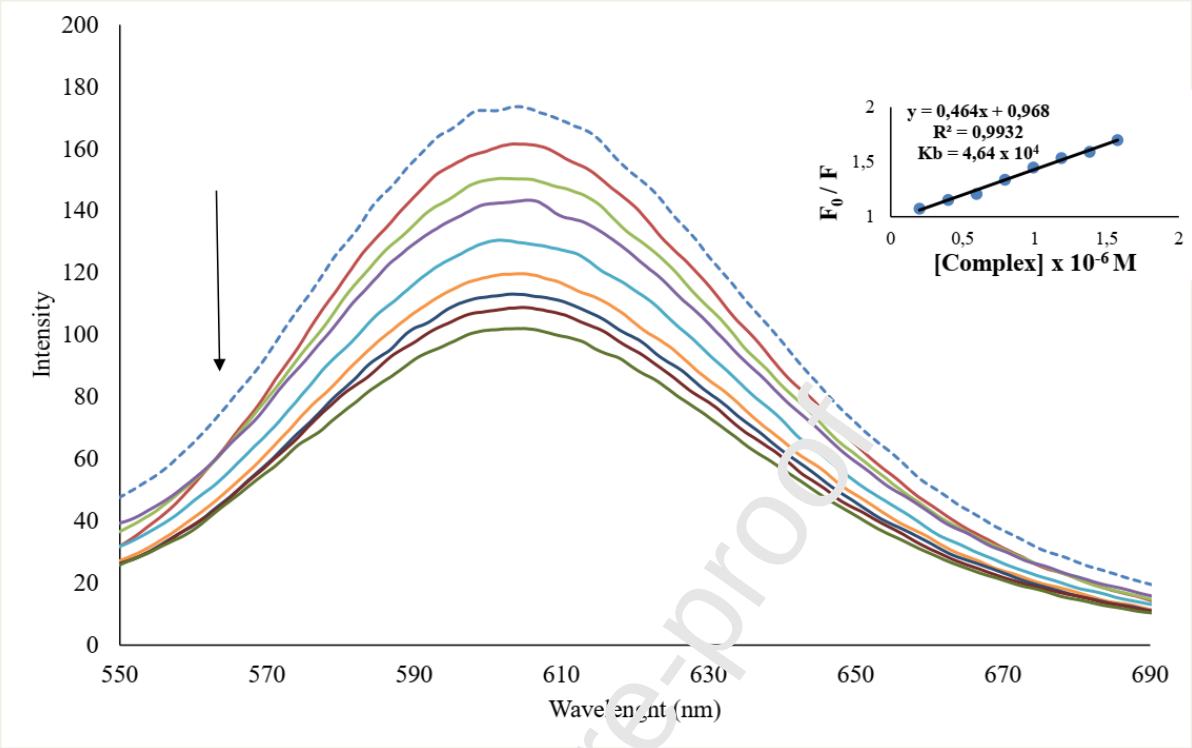

Figure 5a: Fluorescence spectra of EB-CT-DNA in the absence (dashed line) and the presence of a different concentration of complex **8**. (inset) The stern-Volmer plot of **8** interaction with EB-CT-DNA.

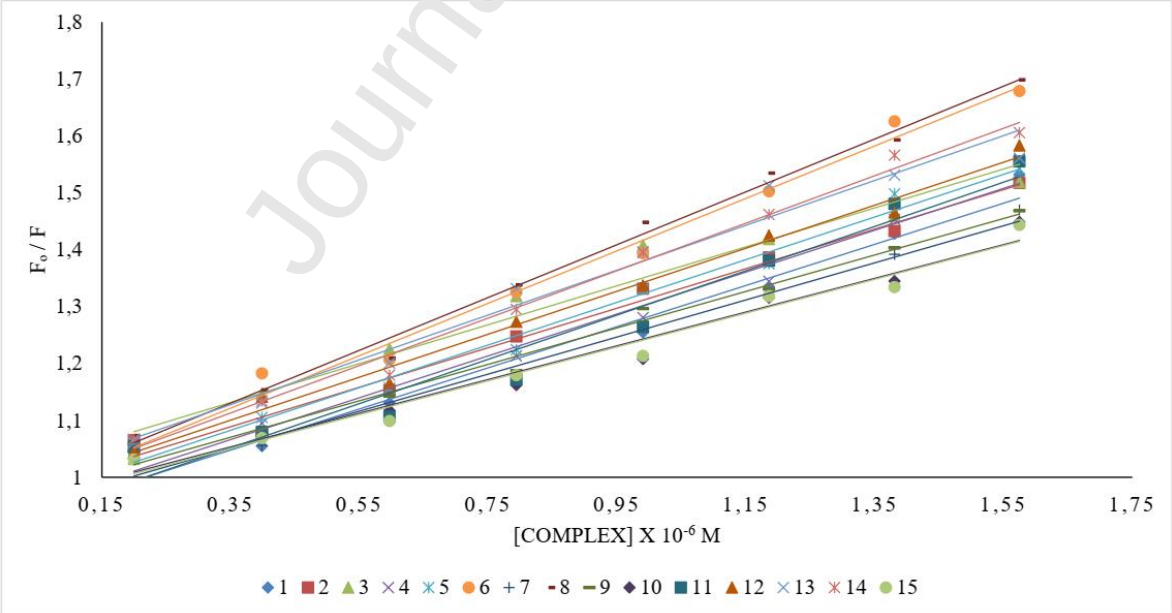

Figure 5b: Stern-Volmer plot of Complexes **1-15** interaction with EB-CT- DNA

Journal Pre-proof

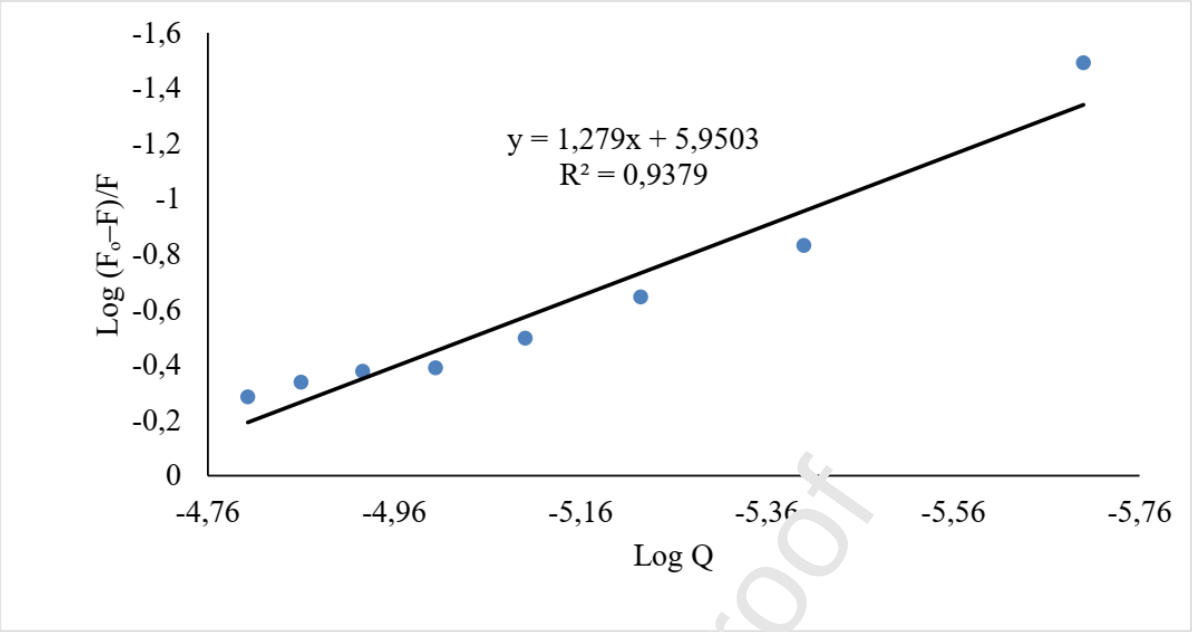

Figure 5c: The double-logarithmic plot of Complex **3**.

3.4.4 *Albumin binding studies using absorption spectroscopy titration*

Serum albumin is an important protein found in the blood plasma and serves as a good carrier of protein for drug molecules. For this reason, protein-binding studies of **1** to **15** are an essential way of studying the compounds metabolism *in vivo*. Bovine serum albumin (BSA) was used as the protein standard in this study because of its close resemblance to human serum albumin (HSA). Absorption spectroscopy titration is a known method used in studying the conformational changes in proteins, and this protein is characterized by an intense absorbance peak at 280 nm depicting the microenvironment around tyrosine and tryptophan residue polarity [80]. On each addition of various concentrations of complexes **1 – 15** to a constant BSA concentration, the intensity of the BSA absorbance intensified between 260 and 300 nm while not showing any shifts (Fig. S50-S63). This is an indicator of some binding interactions between the complexes and BSA. K_b in this instance was determined from the intercept to the slope ratio of the linear curve of a plot of 1/[A-A°] vs. 1/[complex] (inset Fig. S50-S63). The K_b of all the complexes except for **1**, **4, 6** and **11** were in the range of 1.58 x 10^4 – 2.17 x 10^5 M^{-1} (Table 4) which are in conformation with reported related BSA binding constants, normally between 10^4 and 10^6 M^{-1} [46]. This range is a recognized range for drug-carrier complexes. Complexes **1** (K_b = 2.46 x 10^3 M^{-1}), **4** (K_b = 4.21 x 10^3 M^{-1}), **6** (K_b = 5.53 x 10^3 M^{-1}) and 11 (K_b = 6.60 x 10^3 M^{-1}) have K_b values that are lower (hence lower

highest binding affinity (Fig. 6) and those of **3** (Fig. S52) and **13** (Fig. S61) are also high. Their high binding affinity could be a result of high lipophilic interaction of the fluorine substituent in **3, 8** and **13** with protein [81] and the effect of perchlorate anion could have enhanced **8** binding affinity among others. The order of binding constant for the complexes is: **8** > **3** > **13** > **5** > **15** > **10** > **9** > **7** > **2** > **12** > **14** > **11** > **6** > **4** > **1**.

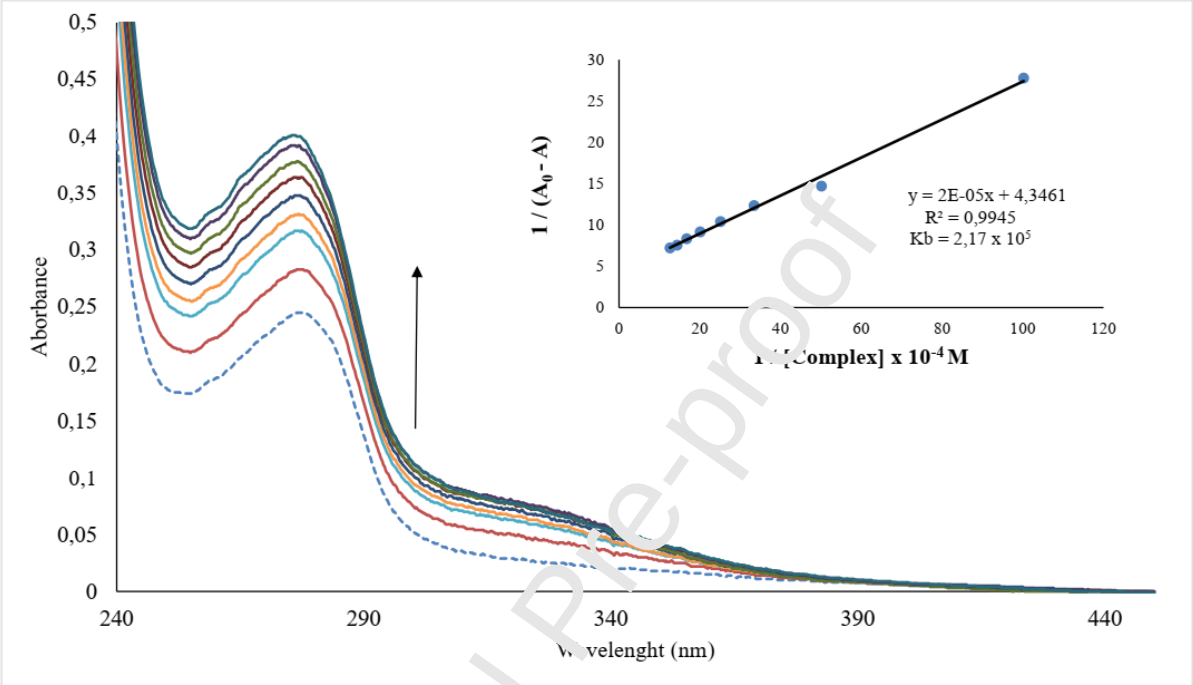

Figure 6: Electronic Absorption Spectra of BSA in the absence (dashed line) and the presence of different concentrations of complexes **8**. (inset) Plot of $1/(A_o - A)$ vs. $1/[Complex] \times 10^{-4}\ M^{-1}$.

3.4.4.1 Fluorescence quenching of bovine serum albumin in the presence of complexes 1 – 15

The fluorescence quenching of protein can provide information on protein binding mechanisms, modes of interaction, and the rates of interaction with drugs or complexes of study [46]. When BSA is excited at 280 nm, it fluoresces strongly between 300 and 400 nm leading to excitation in tyrosine (Tyr) and tryptophan (Trp) residues in proteins. In the presence of a small molecule, BSA has the possibility of undergoing different types of interactions such as hydrophobic, hydrogen bonding, van der Waals, and electrostatic interactions. The ability of a complex to quench BSA fluorescence intensity depends on the hydrophobic interaction between the Trp and the hydrophobic ligand of a complex. The interaction is either enhanced or stabilized by the surrounding amino acid residues [82].

12, **13** and **15** the BSA fluorescence intensity reduces gradually as the concentration of the complexes increases (Fig. S64-S71). The reduction in the fluorescence intensity is accompanied by a slight redshift of the emission wavelength between 1 and 8 nm. This shows that the interaction of **2**, **3**, **5**, **7**, **8**, **10**, **12**, **13** and **15** with BSA causes a conformational change in the protein structure [45]. Furthermore, an isosbestic point between 355 and 387 nm in the spectra of the complex-BSA interaction was observed implying the formation of a stable complex-protein complex. **7** (Fig. 7a) quenched the intrinsic fluorescence of BSA more than the other complexes. The quenching mechanism of the complexes was evaluated using the Stern-Volmer Equation (Eq. **5**).

K_{sv} values for the complexes were obtained from the slope of the plot of I_0/I vs. [Q] and found to be between 1.82 x 10^4 and 1.26 x 10^5 M^{-1}. The calculated values of K_{sv} and K_q for the interaction of the complexes with BSA are given in Table 3. The linearity of the Stern Volmer plots (inset Fig. S64-S71) is an indicator of either a static or a dynamic quenching mechanism. The K_q values obtained for the complexes are between 1.82 x 10^{12} and 1.26 x 10^{13} $M^{-1}S^{-1,}$ which are greater than the maximum scatter collision-quenching constant of biomacromolecules (2 x 10^{10} M^{-1} S^{-1}). This indicates that the interactions between the complexes and BSA are static. Therefore, the binding constant (K_{bin}) and the number of binding sites (n) can be determined using Scatchard Equation **9**:

$$\log \frac{I_o - I}{I} = \log K_{bin} + n\log[Q] \qquad (9)$$

The n and K_{bin} can be calculated from the slope and the intercept of the double logarithm regression curve of $\log(I_o - I)/I$ versus log[Q] (Fig. S78-S85). The values of binding constant (K_{bin}) suggest BSA has a moderate binding affinity to the complexes. Complex **10** (Fig. 7b) has the highest binding affinity to BSA. The number of the binding site (n) for **2**, **3**, **5**, **7**, **8**, **10**, **12**, **13** and **15** is approximately one; this suggests that one molecule of the complexes bound per bovine serum albumin.

The binding constant values show that the complexes can be stored in protein and can be easily released in desired target areas since the values fall within 10^4 - 10^6 $M^{-1,}$ which is the recognized values of non-covalent interaction of BSA with drugs [22]. Complex 8 (Fig. S77) exhibited an extremely low binding constant; this means there is a weak binding interaction of the complex with BSA, which would lead to poor distribution in the blood plasma.

On the contrary, complexes **4**, **9** and **14** only quenched the intrinsic fluoresce of BSA at 1uM concentration after which the intensity of the fluorescence starts increasing with a redshift as

quench the intrinsic fluorescence of BSA (Fig. S72-S77). The BSA fluorescence intensity increased gradually with a redshift as the concentration of the complexes **1**, **6** and **11** was increased. This could be a result of the presence of CH_3 or OH^- substituents in complexes **1**, **4**, **6**, **9**, **11** and **14** ligands. BSA has two tryptophan residues; Try-134 and Trp-213 found in subdomain IB and IIA respectively and are both sensitive to their local environment [83]. Trp-134 has a polar amino acid (Serine) in its environment; therefore, there is the possibility of H-bonding interaction between Trp-134 and the complexes **1**, **6** and **11** OH^- substituent together with the H-bonding involving Tyr or Trp in BSA. This H-bonding interaction is stronger than any other π—π interaction that might have also taken place between the complexes and the Tyr or Trp in BSA. Therefore, the strong hydrophilic interaction between **1**, **6** and **11** and BSA predominate, which in turn leads to the inability of complexes quenching BSA fluorescence. This is in agreement with similarly reported complex [82].

Complexes **4**, **9** and **14** inability to quench BSA further after the addition of 1 µM could not be ascertained but it might be due to the presence of methyl substituent. These complexes' weak interaction with BSA is most likely due to the low hydrophilicity of the ligands in these complexes.

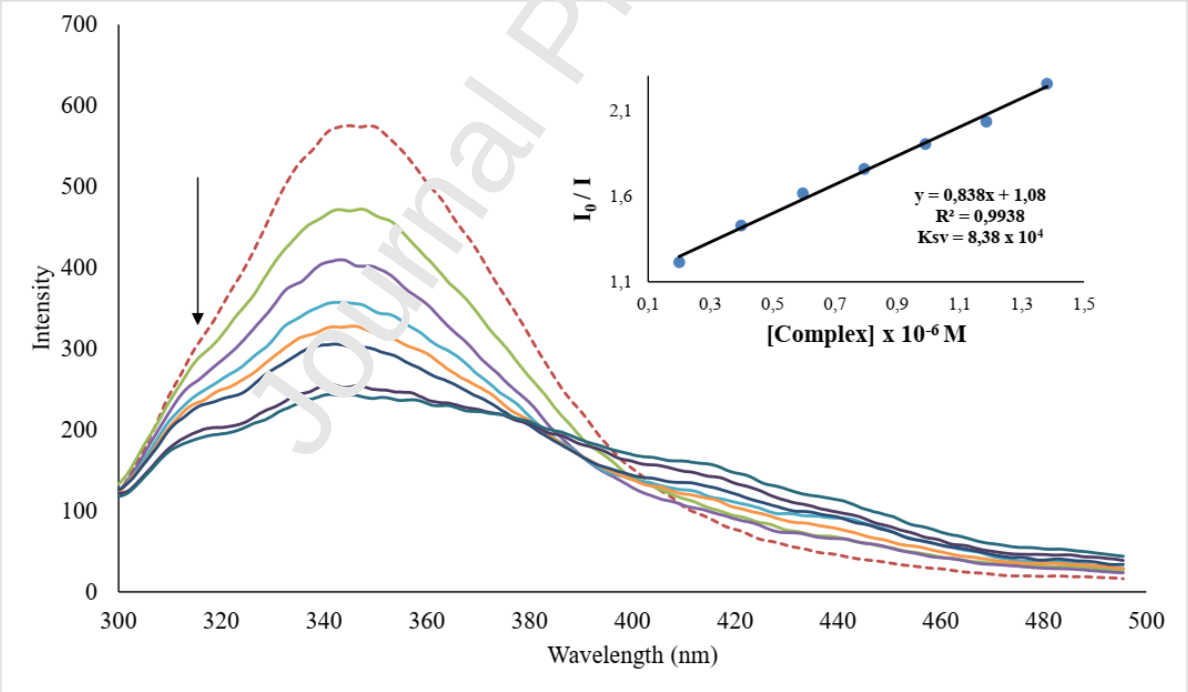

Figure 7a: Fluorescence emission spectra of BSA in the absence(dashed line) and the presence of a different concentration of complex **7**. Inset: A Stern-Volmer plot of the interaction of **7** with BSA.

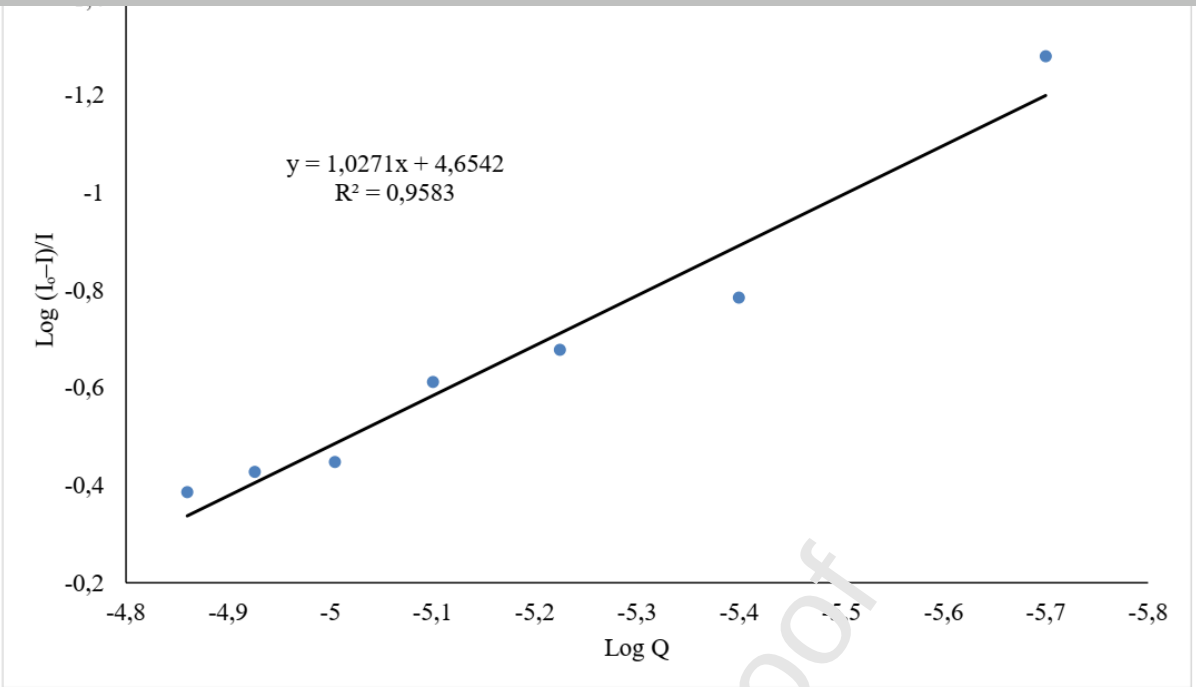

Figure 7b: The double-logarithmic plot of BSA–Complex **10** interactions.

4.0 Conclusion

Five bidentate pyridinyl Schiff bases and their silver(I) complexes were successfully synthesized in a reasonable percentage yield. The antibacterial assay showed the complexes' moderate to high antibacterial activities against MRSA, *S. aureus*, *E. coli*, *S. typhi*, *K. pneumoniae*, and *P. aeruginosa* bacteria. Enhanced antibacterial activities were recorded for complexes with OH^-, F^-, thiazole and thiophene substituents or moiety and ClO_4^- anion in all the bacterial. Similar complexes reported with high antibacterial activity were also observed to have demonstrated excellent antioxidant activity, especially in reducing ferric ion (FRAP). This indicates the compounds' substituent ability to scavenge free radicals by donating electrons rather than a proton. The interaction of the studied complexes with CT-DNA suggests it occurs via intercalation. The relatively moderate to high intrinsic K_b and K_{sv} values obtained from the photophysical studies for the complexes confirmed that Ag(I) pyridinyl Schiff base complexes possess the ability to interact with DNA and only complexes containing hydrophobic ligand can interact with the protein in the blood plasma. The extent of the compounds-protein complex formation determines their distribution in blood plasma since weak binding of compound leads to a shorter lifetime or poor distribution, while strong binding of the compound decreases the concentration of free drug in plasma. With the significant antibacterial, antioxidant, BSA, and DNA binding activities recorded in this study, silver(I) pyridinyl complexes exhibit a good platform for therapeutic drug design.

Abbreviations

BSA	bovine serum albumin
CT-DNA	calf-thymus deoxyribonucleic acid
DMSO	dimethyl sulfoxide
DNA	deoxyribonucleic acid
DPPH	2,2-diphenyl-1-picrylhydrazyl
EB	ethidium bromide
FRAP	ferric reducing antioxidant power
IC_{50}	50 % inhibitory concentration
MHA	müeller-hinton agar
MIC	minimum inhibitory concentration
MRSA	methicillin-resistant staphylococcus aureus
NB	nutrient broth
RNA	ribonucleic acid
ROSs	reactive oxygen species
TPTZ	tripyridyltriazine
Trp	tryptophan
Tyr	tyrosine

Acknowledgements:

Ms Adesola A. Adeleke acknowledges Olabisi Onabanjo University, Ago-Iwoye, for granting her study leave to pursue the PhD programme at the University of KwaZulu-Natal. The authors would like to appreciate the University of KwaZulu-Natal and the National Research Foundation of South Africa (Grant number: 119342) for their financial assistance for Ms Adesola A. Adeleke.

Disclosure statement

No potential conflict of interest was reported by the authors.

Supplementary data

CCDC 2000044-2000048 contain the supplementary crystallographic data for complexes **4**, **5**, **8, 9** and 1**5** respectively. These data can be obtained free of charge via http://www.ccdc.cam.ac.uk/conts/retrieving.html, or from the Cambridge Crystallographic Data Centre, 12 Union Road, Cambridge CB2 1EZ, UK; fax: (+44)1223-336-033; or via e-mail: deposit@ccdc.cam.ac.uk.

References

1. Nur Amin Bitu, M., *Anti-pathogenic Activity of Cu(II) Complexes Incorporating Schiff Bases: A Short Review.* J. Heterocycl. Chem., 2019. **5**(1): p. 11.
2. Belen'kii, L.I., Gramenitskaya, V.N., Evdokimenkova, Y.B., *The Literature of Heterocyclic Chemistry, Part IX, 2002–2004.* Adv. Heterocycl. Chem., 2006. **92**: p. 145-258.
3. Steel, P.J., *Ligand design in multimetallic architectures: six lessons learned.* Acc. Chem. Res., 2005. **38**(4): p. 243-250.
4. Gordeev, M.F., Patel, D.V., Wu, J., Gordon, E.M., *Approaches to combinatorial synthesis of heterocycles: Solid phase synthesis of pyridines and pyrido [2, 3-d] pyrimidines.* Tetrahedron letters, 1996. **37**(27): p. 4643-4646.
5. Abdou, S., Abd-El Wahed, Moshira M., Abu-Setta, Mohammed H.H, *Metallo-Bioactive Compounds as Potential Novel Anticancer Therapy.* IJAC, 2018. **4**(1): p. 17-37.
6. Hussein Eissa, H., *Synthesis, Characterization, Anticorrosion Activity and Antibacterial Activity of Macrocyclic Schiff Bases Based on 1,3-Dithiocarbonyl Phenyl Dihydrazide.* Org. Chem.: Curr. Res., 2016. **04**(04).
7. Shukla, S. and A.P. Mishra, *Synthesis, Structure, and Anticancerous Properties of Silver Complexes.* J. Chem., 2013. **2013**.
8. Gallagher, J.J., Williams-Bouyer, N., Villarreal, C., Heggers, J. P., Herndon, D. N., *Treatment of infection in burns.* Total Burn Care. Philadelphia: Elsevier, Inc, 2007: p. 136-176.
9. Zhang, H., Xu, Y., Wu, H., Aderinto, S. O. Fan, X., *Mono-, bi- and multi-nuclear silver complexes constructed from bis(benzimidazole)-2-oxapropane ligands and methacrylate: syntheses, crystal structures, DNA-binding properties and antioxidant activities.* RSC Advances, 2016. **6**(87): p. 83697-83708.
10. Wu, H., Xia, L., Qu, Y., Zhao, K., Wang, C., Wu, Y., *Synthesis, structure, luminescence and electrochemical and antioxidant properties of anion-controlled silver(I) complexes with 2,2'-(1,4-butanediyl)bis-1,3-benzoxazole.* Applied Organometallic Chemistry, 2019. **34**(1).
11. Tang, X., Qu, Y., Zhao, K., Wang, C., Wu, Y., Mao, S., Wu, H., *Synthesis, crystal structure, fluorescence and antioxidant properties of a binuclear Ag(I) complex based on the SPPh3 ligand.* Journal of Chemical Research, 2019. **43**(5-6): p. 184-188.
12. Thornton, L., Dixit, V., Assaf, L. O. N., Ribeiro, T. P., Queiroz, D. D., Kellett, A., Casey, A., Colleran, J., Pereira, M. D., Rochford, G., McCann, M., O'Shea, D., Dempsey, R., McClean, S., Kia, A. F., Walsh, M., Creaven, B., Howe, O., Devereux, M., *Water-soluble and photo-stable silver(I) dicarboxylate complexes containing 1,10-phenanthroline ligands: Antimicrobial and anticancer chemotherapeutic potential, DNA interactions and antioxidant activity.* Journal of Inorganic Biochemistry, 2016. **159**: p. 120-132.
13. Oladipo, S.D., Mocktar, C., Omondi, Bernard, *In vitro biological studies of heteroleptic Ag(I) and Cu(I) unsymmetrical N,N'-diarylformamidine dithiocarbamate phosphine complexes; the effect of the metal center.* Arabian Journal of Chemistry, 2020.
14. Somayeh M., K., M. F., Rajabi, H. R., Pourmortazavi, S. M., *Green and Simple Synthesis of Silver Nanoparticles by Aqueous Extract of Perovskia abrotanoides: Characterization, Optimization and Antimicrobial Activity.* Current Pharmaceutical Biotechnology, 2019. **20**: p. 1-9.
15. Wang, K., Wu, Y., Li, H., Li, M., Guan, F., Fan, H., *A hybrid antioxidizing and antibacterial material based on Ag-La2O3 nanocomposites.* J Inorg Biochem, 2014. **141**: p. 36-42.
16. Movahedi, E., Rezvani, A.R., *Multispectroscopic DNA-Binding studies and antimicrobial evaluation of new mixed-ligand Silver(I) complex and nanocomplex: A comparative study.* Journal of Molecular Structure, 2018. **1160**: p. 117-128.
17. Phaniendra, A., Jestadi, D.B., Periyasamy, L., *Free radicals: properties, sources, targets, and their implication in various diseases.* Indian J Clin Biochem, 2015. **30**(1): p. 11-26.
18. Movahedi, E., Rezvani, A.R., *New silver(I) complex with diazafluorene based ligand: Synthesis, characterization, investigation of in vitro DNA binding and antimicrobial studies.* J. Mol. Struct., 2017. **1139**: p. 407-417.

by small molecules. Beilstein J. Org. Chem., 2018. **14**(1): p. 1051-1086.
20. Nanjunda, R., Wilson, W. D., *Binding to the DNA Minor Groove by Heterocyclic Dications: From AT-Specific Monomers to GC Recognition with Dimers.* Curr. protoc. nucleic acid chem., 2012. **51**(1): p. 8.8.1-8.8.20.
21. Kellett, A., Molphy, Z., Slator, C., McKee, V., Farrell, N. P., *Molecular methods for assessment of non-covalent metallodrug–DNA interactions.* Chemical Society Reviews, 2019. **48**(4): p. 971-988.
22. Hong, M., Geng, H., Niu, M., Wang, F., Li, D., Liu, J., Yin, H., *Organotin(IV) complexes derived from Schiff base N'-[(1E)-(2-hydroxy-3-methoxyphenyl)methylidene]pyridine-4-carbohydrazone: synthesis, in vitro cytotoxicities and DNA/BSA interaction.* Eur. J. Med. Chem., 2014. **86**: p. 550-61.
23. Jehdaramarn, A., Pornsuwan, S., Chumsaeng, P., Phomphrai, K., Sangtrirutnugul, P., *Effects of appended hydroxyl groups and ligand chain length on copper coordination and oxidation activity.* New Journal of Chemistry, 2018. **42**(1): p. 654-661.
24. Carlson, L.J., Welby, J., Zebrowski, K.A., Wilk, M.M., Giroux, R., Ciancio, N., Tanski, J.M., Bradley, A., Tyler, L.A., *Spectroscopic differences between heterocyclic benzothiazoline, -thiazole and imine containing ligands and comparison of the Co and Cu pyridine benzothiazole and imine complexes.* Inorganica Chimica Acta, 2011. **365**(1): p. 159-166.
25. Koske, M.C., Kagwanja, S.M., Gichumbi, J.M., Kariuki, S.M., *Synthesis, Characterization, Electrochemical and Antibacterial Studies of Half-sandwich Ru (II) Complex of 4-fluoro-N-(2-pyridiylmethylene)-aniline Schiff Base.*
26. Al-Rashdi, K.S., Al-Khathami, N.D., Basaleh, A.S., Al-Jandali, M., Babgi, B.A., Eltayeb, N.E., *Synthesis of Novel Pyridyl-Based Schiff Base and Its Coordination Behaviour with Ruthenium (II) and Zinc (II).* Asian Journal of Chemistry, 2017. **29**(8).
27. Spinu, C., Pleniceanu, M., Tigae, C., *Biologically active transition metal chelates with a 2-thiophenecarboxaldehyde-derived Schiff base: synthesis, characterization, and antibacterial properties.* Turkish Journal of Chemistry, 2008. **32**(4): p. 487-493.
28. Ali, O.A.M., El-Medani, S.M., Ahmed, E.A., Nassar, D.A., *Metal carbonyl complexes with Schiff bases derived from 2-pyridinecarboxaldehyde: Syntheses, spectral, catalytic activity and antimicrobial activity studies.* Journal of Molecular Structure, 2014. **1074**: p. 713-722.
29. Njogu, E.M., Omondi, B., Nyamori, V. O., *Silver(I)-pyridinyl Schiff base complexes: Synthesis, characterisation and antimicrobial studies.* J. Mol. Struct., 2017. **1135**: p. 118-128.
30. SAINT, B., *Data reduction software.* Bruker AXS Inc., Madison, Wisconsin, USA, 2009.
31. Bruker, A., *Saint and SADABS.* Bruker AXS Inc., Madison, Wisconsin, USA, 2009.
32. Sheldrick, G.M., *Crystal structure solution with ShelXT.* Acta Crystallogr. A, 2015. **71**: p. 3-8.
33. Farrugia, L., *WinGX and ORTEP for Windows: an update.* J. Appl. Cryst., 2012. **45**(4): p. 849-854.
34. Sheldrick, G., *A short history of SHELX.* Acta Crystallographica Section A, 2008. **64**(1): p. 112-122.
35. Spek, A.L., *PLATON SQUEEZE: a tool for the calculation of the disordered solvent contribution to the calculated structure factors.* Acta Crystallogr C Struct Chem, 2015. **71**(Pt 1): p. 9-18.
36. Spek, A.L., *Platon: A Multipurpose Crystallographic Tool, version 1.17; Utrecht University: Utrecht, The Netherlands.* 2013.
37. Oladipo, S.D., Omondi, B., Mocktar, C., *Synthesis and structural studies of nickel(II)- and copper(II)-N,N'-diarylformamidine dithiocarbamate complexes as antimicrobial and antioxidant agents.* Polyhedron, 2019. **170**: p. 712-722.
38. Nayak, S.G., Poojary, B., *Synthesis of novel Schiff bases containing arylpyrimidines as promising antibacterial agents.* Heliyon, 2019. **5**(8): p. e02318.
39. Njogu, E.M., Martincigh, B. S., Omondi, B., Nyamori, V. O., *Synthesis, characterization, antimicrobial screening and DNA binding of novel silver(I)-thienylterpyridine and silver(I)-furylterpyridine complexes.* Appl. Organomet. Chem., 2018. **32**(12): p. e4554.
40. Liyana-Pathirana, C.M., Shahidi, F., *Antioxidant activity of commercial soft and hard wheat (Triticum aestivum L.) as affected by gastric pH conditions.* J. Agric. Food Chem., 2005. **53**(7): p. 2433-2440.

Activity and Ferric Reducing Ability of Juniperus thurifera (L.), J. oxycedrus (L.), J. phoenicea (L.) and Tetraclinis articulata (L.). Adv. Pharmacol. Sci., 2016. **2016**: p. 6392656.

42. Raman, N., Sakthivel, A., Jeyamurugan, R., *Synthesis, characterization, DNA binding, photo-induced DNA cleavage, and antimicrobial activity of metal complexes of a Schiff base derived frombis(3-aminophenyl)malonamide.* J. Coord. Chem., 2009. **62**(24): p. 3969-3985.
43. Abdel-Rahman, L.H., Abu-Dief, Ahmed M., El-Khatib, R.M., Abdel-Fatah, S.M., Seleem, A. A., *New Cd(II), Mn(II) and Ag(I) Schiff Base Complexes : Synthesis, Characterization, DNA Binding and Antimicrobial Activity.* IJNC, 2016. **2**(3): p. 83-91.
44. Vamsikrishna, N., Kumar, M.P., Ramesh, G., Ganji, N. Daravath, S., Shivaraj, *DNA interactions and biocidal activity of metal complexes of benzothiazole Schiff bases: synthesis, characterization and validation.* J. Chem. Sci., 2017. **129**(5): p. 609-622.
45. Gomathi, A., Vijayan, P., Viswanathamurthi, P., Suresh, S., Nandhakumar, R., Hashimoto, T., *Organoruthenium(II) compounds with pyridyl benzoxazole/benzthiazole moiety: studies on DNA/protein binding and enzyme mimetic activities.* J. Coord. Chem., 2017. **70**(10): p. 1645-1666.
46. Anjomshoa, M., Fatemi, S.J., Torkzadeh-Mahani, M., Hadadzadeh, H., *DNA- and BSA-binding studies and anticancer activity against human breast cancer cells (MCF-7) of the zinc(II) complex coordinated by 5,6-diphenyl-3-(2-pyridyl)-1,2,4-triazine.* Spectrochim Acta A Mol Biomol Spectrosc, 2014. **127**: p. 511-520.
47. Lee, Y.J., Lee, S.W., *Ligands containing pyridyl-carboxylate terminals and their discrete silver and polymeric cadmium compounds: (n-py)–CHN–$C_{10}H_6$–COOH (n=2 (HL^1), 3(HL^2)), [$Ag(HL^1)_2$](PF_6), [$Ag(HL^1)_2$](NO_3)(H_2O), and [$Cd(L^2)_2$].* Polyhedron, 2013. **53**: p. 103-112.
48. Huang-Chun Wu, P.T., Chi-Hwe Tsai, Jing-Yun Wu, Sheng-Ming Huang, Yuh-Sheng Wen., Kuang-Lieh L., *Self-Assembly, Reorganization, and Photophysical Properties of Silver(I)−Schiff-Base Molecular Rectangle and Polymeric Array Species.* Inorg. Chem., 2006. **45**(1): p. 295−303.
49. Pucci, D., Barberio, G., Bellusci, A., Crispini, A., La Deda, M., Ghedini, M., Szerb, E. I., *Induction of Columnar Mesomorphism in Tetracoordinated Ionic Silver(I) Complexes Based on Chelate 4,4'-Disubstituted 2,2'-Bipyridines.* Eur. J. Inorg. Chem., 2005. **2005**(12): p. 2457-2463.
50. Li, H., Liu, C., Dai, B., Tang, X., Zhang, Z. J., Xiong, Z., Liu, X., *Synthesis, conductivity, and electromagnetic wave absorption properties of chiral poly Schiff bases and their silver complexes.* J. Appl. Polym. Sci., 2015. **132**(36).
51. Dehghanpour, S., Mahmoudi, A., *Synthesis, structure, and redox properties of copper(I) complexes with phenylpyridin-2-ylmethyleneamine derivatives.* Main Group Chem., 2007. **6**(2): p. 121-130.
52. Vallejos, J., Brito, I., Cardenas, A., Bolte, M., Conejeros, S., Alemany, P., Llanos, J., *Self-Assembly of Discrete Metallocycles versus Coordination Polymers Based on Cu(I) and Ag(I) Ions and Flexible Ligands: Structural Diversification and Luminescent Properties.* Polymers (Basel), 2016. **8**(46).
53. Njogu, E.M., Omondi, B., Nyamori, V. O., *Synthesis, physical and antimicrobial studies of ferrocenyl-N-(pyridinylmethylene)anilines and ferrocenyl-N-(pyridinylmethyl)anilines.* S. Afr. J. Chem., 2016. **69**: p. 51-66.
54. Njogu, E.M., Omondi, B., Nyamori, V. O., *Coordination polymers and discrete complexes of Ag(I)-N-(pyridylmethylene)anilines: synthesis, crystal structures and photophysical properties.* J. Coord. Chem., 2017. **70**(16): p. 2796-2814.
55. Njogu, E.M., Omondi, B., Nyamori, V. O., *Silver(I)-pyridinyl Schiff base complexes: Synthesis, structural characterization and reactivity in ring-opening polymerisation of ε-caprolactone.* Inorganica Chimica Acta, 2017. **457**: p. 160-170.
56. Yang, L., D.R. Powell, and R.P. Houser, *Structural variation in copper(I) complexes with pyridylmethylamide ligands: structural analysis with a new four-coordinate geometry index, tau4.* Dalton Trans., 2007(9): p. 955-64.

complexes derived from aryl-benzothiazoles as turn-on sensors: Syntheses, properties and density functional studies. Inorganica Chimica Acta, 2018. **471**: p. 326-335.
58. Raj, P., Singh, A., Singh, A., Singh, N., *Syntheses and Photophysical Properties of Schiff Base Ni(II) Complexes: Application for Sustainable Antibacterial Activity and Cytotoxicity.* ACS Sustain. Chem. Eng., 2017. **5**(7): p. 6070-6080.
59. Abou-Hussein, A.A. and W. Linert, *Synthesis, spectroscopic, coordination and biological activities of some organometallic complexes derived from thio-Schiff base ligands.* Spectrochim Acta A Mol Biomol Spectrosc, 2014. **117**: p. 763-771.
60. Aldabaldetrecu, M., Tamayo, L., Alarcon, R., Walter, M., Salas-Huenuleo, E., Kogan, M.J., Guerrero, J., Paez, M., Azocar, M. I., *Stability of Antibacterial Silver Carboxylate Complexes against Staphylococcus epidermidis and Their Cytotoxic Effects.* Molecules, 2018. **23**(7).
61. Shah, R. and P.K. Verma, *Therapeutic importance of synthetic thiophene.* Chem Cent J, 2018. **12**(1): p. 137.
62. Raman, N., Joseph, J., Sakthivel, A. Jeyamurugan, R., *Synthesis, structural characterization and antimicrobial studies of novel Schiff base copper (II) complexes.* J. Chil. Chem. Soc., 2009. **54**(4): p. 354-357.
63. Carreira-Barral, I., Rumbo, C., Mielczarek, M., Alonso-Carrillo, D., Herran, E., Pastor, M., Del Pozo, A., Garcia-Valverde, M., Quesada, R., *Small molecule anion transporters display in vitro antimicrobial activity against clinically relevant bacterial strains.* Chem Commun (Camb), 2019. **55**(68): p. 10080-10083.
64. Wu, H., Yuan, J., Bai, Y., Pan, G., Wang, H., Kong, J., Fan, X., Liu, H., *Synthesis, structure, DNA-binding properties and antioxidant activity of silver(I) complexes containing V-shaped bis-benzimidazole ligands.* Dalton Trans., 2012. **41**(29): p. 8829-38.
65. Phaniendra, A., Jestadi, D. B., Periyasamy, L. *Free Radicals: Properties, Sources, Targets, and Their Implication in Various Diseases.* Indian Journal of Clinical Biochemistry, 2014. **30**(1): p. 11-26.
66. Santos-Sánchez, N.F., Salas-Coronado, R., Villanueva-Cañongo, C., Hernández-Carlos, B., *Antioxidant compounds and their antioxidant mechanism*, in *Antioxidants*. 2019, IntechOpen.
67. Kavitha, P., Saritha, M. and Laxma Reddy, K., *Synthesis, structural characterization, fluorescence, antimicrobial, antioxidant and DNA cleavage studies of Cu(II) complexes of formyl chromone Schiff bases.* Spectrochim Acta A Mol. Biomol. Spectrosc., 2013. **102**: p. 159-68.
68. Irshad, M., Zafaryab, M., Singh, M., Rizvi, M.M., *Comparative Analysis of the Antioxidant Activity of Cassia fistula Extracts.* Int. J. Med. Chem., 2012. **2012**: p. 157125.
69. Borra, S.K., Gurumurthy, P., Mahendra, J., *Antioxidant and free radical scavenging activity of curcumin determined by using different in vitro and ex vivo models.* Journal of Medicinal Plants Research, 2013. **7**(36): p. 2680-2690.
70. Saravanakumar, A., P. Periyasamy, and H.T. Jang, *In vitro assessment of three different artemisia species for their antioxidant and anti-fibrotic activity.* Biocatalysis and Agricultural Biotechnology, 2019. **18**: p. 101040.
71. Elsayed, S.A., E.A. Saad, and S.I. Mostafa, *Development of new potential anticancer metal complexes derived from 2-hydrazinobenzothiazole.* Mini reviews in medicinal chemistry, 2019. **19**(11): p. 913-922.
72. Mruthyunjayaswamy, B.H.M., Nagesh, G.Y., Ramesh, M., Priyanka, B., Heena, B., *Synthesis, characterization and antioxidant activity of Schiff base ligand and its metal complexes containing thiazole moiety.* 2015.
73. Fadda, A.A., Tawfik, E.H., Selim, Y.A., *Synthesis and Biological Evaluation of Some New Thiophene, Thiazole, Dithiolane Derivatives and Related Compounds.* Polycyclic Aromatic Compounds, 2018: p. 1-14.
74. Banti, C.N., Giannoulis, A. D., Kourkoumelis, N., Owczarzak, A. M., Poyraz, M., Kubicki, M., Charalabopoulos, K. and Hadjikakou, S. K., *Mixed ligand-silver(I) complexes with anti-inflammatory agents which can bind to lipoxygenase and calf-thymus DNA, modulating their function and inducing apoptosis.* Metallomics, 2012. **4**(6): p. 545-60.

terpyridines and naproxen: DNA interaction, EGFR/VEGFR2 kinase, growth inhibition and cell cycle arrest studies. Mater. Sci. Eng. C. Mater. Biol. Appl., 2017. **76**: p. 601-615.

76. Aleksić, M. and V. Kapetanović, *An overview of the optical and electrochemical methods for detection of DNA-drug interactions.* Acta Chimica Slovenica, 2014. **61**(3): p. 555-573.
77. Rendosova, M., Vargova, Z., Kuchar, J., Sabolova, D., Levoca, S., Kudlacova, J., Paulikova, H., Hudecova, D., Helebrandtova, V., Almasi, M., Vilkova, M., Dusek, M. and Bobalova, D., *New silver complexes with bioactive glycine and nicotinamide molecules - Characterization, DNA binding, antimicrobial and anticancer evaluation.* J. Inorg. Biochem., 2017. **168**.
78. Kazemi, Z., Rudbari, H. A., Mirkhani, V., Sahihi, M., Moghadam, M., Tangestaninejad, S., Mohammadpoor-Baltork, I., *Synthesis, characterization, crystal structure, DNA- and HSA-binding studies of a dinuclear Schiff base Zn(II) complex derived from 2-hydroxynaphtaldehyde and 2-picolylamine.* J. Mol. Struct., 2015. **1096**: p. 110-120.
79. Saeidifar, M., Sohrabi Jam, Z., Shahraki, S., Khanlarkhani, A., Javaheri, M., Divsalar, A., Mansouri-Torshizi, H., Akbar Saboury, A., *Multi-spectroscopic and electrochemical approaches of the interaction between a new binuclear agent and DNA.* J. Biomol. Struct. Dyn., 2017. **35**(12): p. 2557-2564.
80. Abeydeera, N., Perera, I.C., Perera, T., *Synthesis, Characterization, and BSA-Binding Studies of Novel Sulfonated Zinc-Triazine Complexes.* Bioinorg Chem Appl, 2018. **2018**: p. 7563820.
81. Bohm, H.J., Banner, D., Bendels, S., Kansy, M., Kuhn, B., Müller, K., Obst-Sander, U., Stahl, M., *Fluorine in medicinal chemistry.* ChemBioChem, 2004. **5**(5): p. 637-43.
82. Crouse, H.F., Potoma, J., Nejrabi, F., Snyder, D.L., Chohan, B. S., Basu, S., *Quenching of tryptophan fluorescence in various proteins by a series of small nickel complexes.* Dalton Trans., 2012. **41**(9): p. 2720-2731.
83. Malarkani, K., Sarkar, I., Selvam, S., *Denaturation studies on bovine serum albumin-bile salt system: Bile salt stabilizes bovine serum albumin through hydrophobicity.* J. Pharm. Anal., 2018. **8**(1): p. 27-36.

Journal Pre-proof

There are no conflicts of interest

Journal Pre-proof

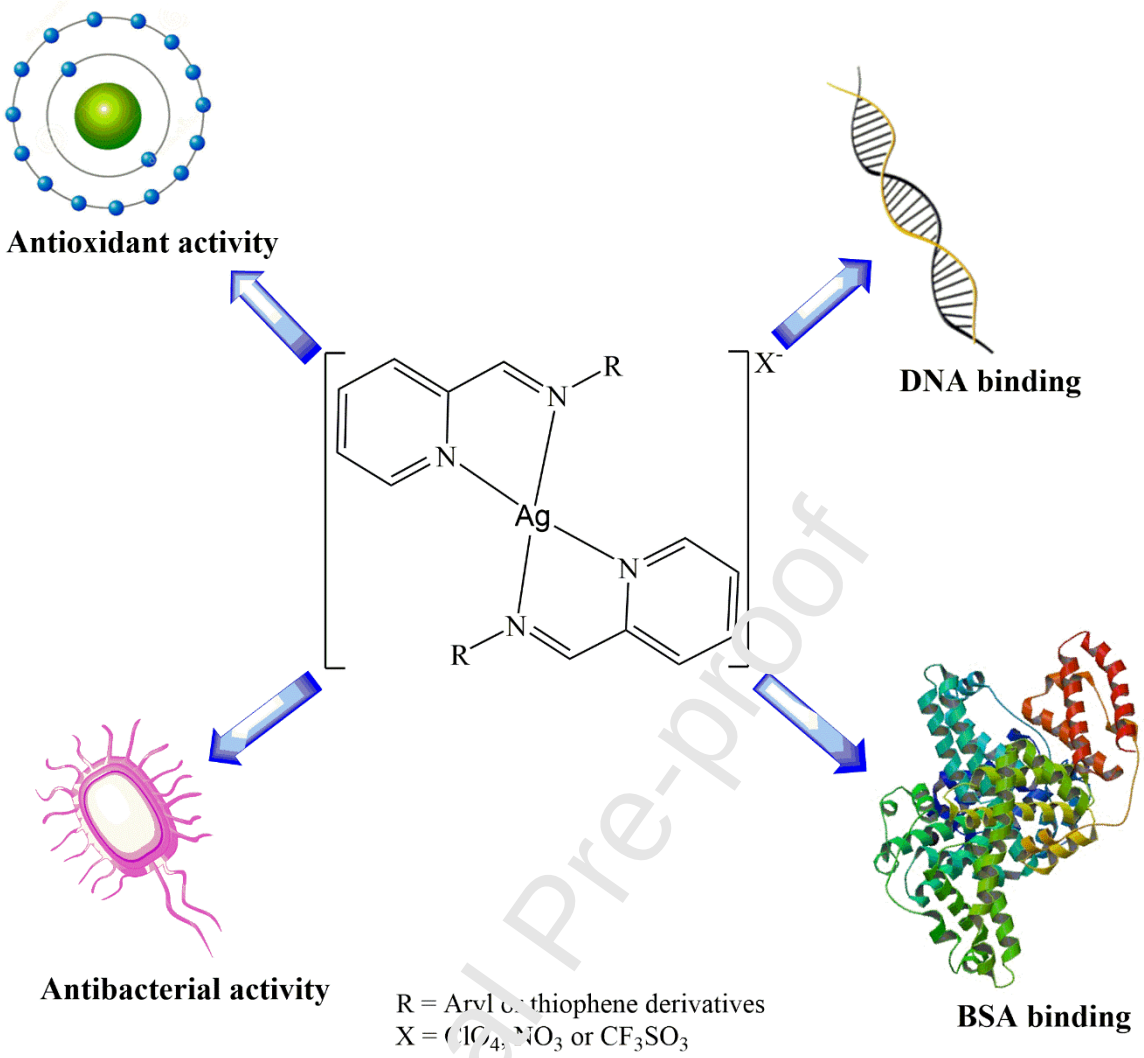

Graphical Abstract Synopsis

Synthesis of pyridinyl silver(I) complexes were prepared and fully characterized. The complexes are potential antibacterial and antioxidant agents. The complexes also showed remarkable interaction with calf thymus deoxyribonucleic acid and bovine serum albumin.

Journal Pre-proof

- Synthesis of discrete pyridinyl imine silver(I) complexes.
- Anion and substituents variation.
- Interaction of pyridinyl silver(I) complexes with calf-thymus deoxyribonucleic acid via intercalation mode.
- The complexes quench the fluorescence of bovine serum albumin through a static mechanism.
- Remarkable antioxidant and antimicrobial activities.

Journal Pre-proof